UNIVERSITÀ DEGLI STUDI DI PADOVA

DIPARTIMENTO DI INGEGNERIA INDUSTRIALE

CORSO DI LAUREA MAGISTRALE IN INGEGNERIA CHIMICA E DEI PROCESSI INDUSTRIALI

Tesi di Laurea Magistrale in

Ingegneria Chimica e dei Processi Industriali

INVESTIGATION OF THE SPINCHEM® ROTATING BED REACTOR: INTERNALLY AND EXTERNALLY MASS TRANSFER LIMITED REACTIONS

Relatore: Prof. Paolo Canu
Correlatore: Prof. Jyri-Pekka Mikkola

Laureando: MAURILIO MAGOSSO

ANNO ACCADEMICO 2014 – 2015

Acknowledgements

I would like to thank first of all prof. Paolo Canu who gave me the great opportunity to make this new exciting life and study experience in Sweden and helped me for the thesis work. Thanks also to prof. Jyri-Pekka Mikkola and Dr. Emil Byström for the interesting thesis topic and the supervision and guidance during the work.

A special thank goes to the other people of the laboratory who assisted me during my project also if they were not involved in it: Ajaikumar and Rakesh Samikannu, Ngoc Tung Pham, Natalia Bukhanko and Ngoc Phuoc Dinh. I feel to express a special gratitude to Ajaikumar Samikannu, not only for his great kindness and his constant availability to help me for the thesis, but also for his friendship and his valuable advices about my future career. How could I forget Anton Tokarev. He always had a solution for all the problems that I encountered during the thesis work and, above all, he was cheerful and ready to talk every time, bringing the joy in the laboratory and in the office.

Abstract

The Thesis is about the study of an innovative reactor: the SpinChem® Rotating Bed Reactor (RBR), developed by the company SpinChem AB. This reactor is conceived for heterogeneous reactions, especially for solid-liquid reactions.
It consists in a rotating stirring element that holds the solid inside, as a packed bed and force a liquid flow through the solids. The flow rate of the liquid in the stirring element is proportional to the rotation speed. This mechanism is expected to improve the solid-liquid external mass transfer, with respect to a normal stirred tank reactor (STR) in which the solid and the liquid are mixed with classical impellers.
In this work the RBR have been compared with a tank reactor stirred by a common impeller. Comparison was carried out at different rotation speeds, using two different solid-liquid non-catalytic reactions: 1) the scavenging of a genotoxic impurity and 2) an ion-exchange reaction. In the first reaction we found that there was no difference between the two mixers because the reaction is not limited by the external mass transfer. Both the chemical kinetics and the internal mass transfer inside the pores of the solids are the slowest steps that control the reaction rate.
On the contrary, the ion-exchange reaction appeared clearly limited by the external mass transfer and the RBR performs better than the STR for the rotation speeds above 400 rpm.

A further study was carried out using the same ion-exchange reaction and the RBR, to investigate the influence of the baffles type and the distance of the rotating bed from the bottom. It was found that both these variables have an effect on the reaction rate and should therefore be taken into account when the RBR is used for kinetic investigations.

Riassunto

Questo lavoro di tesi riguarda lo studio di un nuovo tipo di reattore: il reattore a letto rotante SpinChem® (RBR), sviluppato dall'azienda SpinChem AB. Questo reattore è stato concepito per reazioni multifase e specialmente per reazioni solido-liquido.
Il reattore è costituito da un recipiente dotato di baffles e un elemento rotante (letto rotante) al cui interno è contenuto il solido, come una sorta di letto impaccato. Il liquido viene continuamente risucchiato all'interno del letto rotante e fatto passare attraverso le particelle di solido. Il flusso di liquido attraverso il solido è direttamente proporzionale alla velocità di rotazione del letto rotante. In questo modo il trasferimento di materia esterno tra solido e liquido dovrebbe essere incrementato rispetto ad un normale reattore agitato (STR), nel quale il liquido e il solido disperso vengono mescolati con un comune agitatore.
In questo lavoro lo SpinChem® RBR è stato confrontato con il classico STR, per diverse velocità di rotazione, usando due reazioni solido-liquido non-catalitiche: la rimozione di una impurità genotossica da una soluzione e una reazione di scambio ionico.
La prima reazione è risultata in regime di trasferimento di materia interno (nei pori del solido), per cui non è stata riscontrata alcuna differenza fra i due reattori.
Per quanto riguarda la prima reazione è stato verificato che non v'è differenza tra i due tipi di reattore in quanto la reazione non è limitata dal trasferimento di materia esterno.
É risultato invece che, probabilmente, sia la cinetica che il mass-transfer all'interno dei pori del solido sono gli step più lenti del meccanismo di reazione e controllano quindi la velocità di reazione.
La reazione di scambio ionico era invece in regime di trasferimento di materia esterno e lo SpinChem® RBR è risultato migliore dello STR per velocità di rotazione maggiori di 400 rpm circa.
Sempre utilizzando la reazione di scambio ionico e lo SpinChem® RBR, è stata studiata l'influenza del tipo di baffles e della distanza del letto rotante dal fondo del reattore. È stato trovato che entrambi queste variabili incidono sulla velocità di reazione e dovrebbero essere tenute in conto quando vengono condotti studi di questo tipo.

Table of Contents

Introduction

This thesis work is about the study of a novel type of reactor developed by the company SpinChem AB in Umeå, Sweden: the SpinChem® rotating bed reactor (RBR).
This reactor has been ideated to enhance the external mass transfer in heterogeneous reactions involving solids and/or liquids.
It is an alternative to the normal reactors used for this type of reactions: the stirred tank reactor (STR) and the packed bed reactor (PBR). The working principles of these two reactors are combined together in the SpinChem® RBR. The SpinChem® RBR is a cylinder connected to a rotating shaft; it holds the solid phase as a packed bed and rapidly aspirates the reaction solution from the bottom of the vessel, percolates it through the solid phase and quickly returns it to the vessel.
Since this product is quite new it is of interest to study it deeply and find new applications for which it offers advantages with respect to the normal reactors cited above.
The aim of this work was to test the SpinChem® RBR for two solid-liquid applications: the scavenging of a genotoxic impurity and an ion-exchange reaction.
For both the reactions the RBR was compared, at different rotation speeds, with a normal STR. Furthermore, using the ion-exchange reaction, the influence of some geometrical parameters on the performance of the SpinChem® RBR was investigated. The geometrical parameters studied were: the type of baffles, the position (height) of the rotating bed in the vessel and the diameter of the vessel.
The thesis is divided in five chapters. The first chapter is an overview on the theory about solid-liquid reactions. In Chapter 2 the SpinChem® RBR is described in detail. Chapter 3 is about the study of the first application: the scavenging of a genotoxic impurity. The second application studied, the ion-exchange reaction, is treated in Chapter 4. In the same chapter are also reported the results about the investigation of the importance of the type of baffles, the height of the rotating bed and the vessel diameter in the SpinChem® RBR. In the last chapter, Chapter 5, there are the conclusions of the work.

Chapter 1

Solid-liquid heterogeneous reactions

In the thesis work two different solid-liquid heterogeneous non-catalytic reactions have been investigated. Though the chemistry of these reactions is different, they both belong to the same category and are governed by the same mechanisms.
A liquid species (A) is removed from the bulk of the liquid solution, where it is initially present, by reaction with a porous solid (S). This solid is made of an inert substrate (i.e. fused silica gel or polymer) whose surface is functionalized with the desired reactive functional groups (X). Thus the reaction take place at the surface of the solid and after it the liquid molecules that have to be removed are permanently linked to the functional groups of the solid, which can be separated from the clean solution when the desired purity is achieved.
The scheme of the reaction is depicted in Fig. 1.

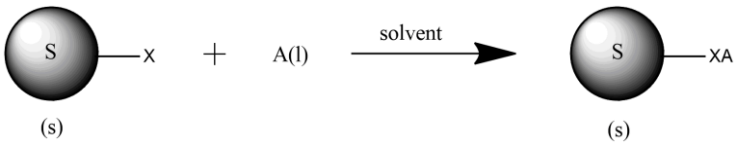

Figure 1.1. *General scheme of the solid-liquid reactions studied in the thesis work*

In this chapter the theoretical aspects regarding solid-liquid heterogeneous reactions of this type that will be useful in this study are presented.

1.1 Mechanisms involved in solid-liquid heterogeneous reactions

In solid-liquid mass transfer processes, the rate-controlling steps, as depicted in Fig. 1.2 are:

- diffusion in the liquid film surrounding the solid particles (film diffusion or external mass transfer);
- diffusion within the particle pores or through the solid phase itself (particle diffusion or internal mass transfer);
- chemical reaction at the surface of the particle (surface reaction).

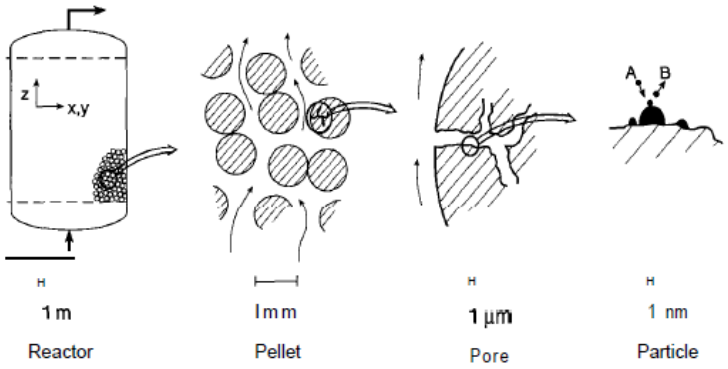

Figure 1.2. *Different size scales in a heterogeneous solid-liquid reactor. From the flow around catalyst pellets to diffusion within pores of pellets and reaction on reaction sites. These span distance scales from meters to Angstroms. Adapted from Schmidt, 1998.*

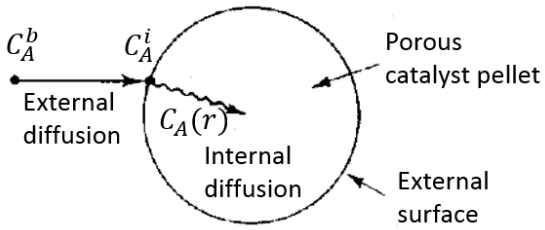

Figure 1.3. *Mass transfer and reaction steps in a solid particle. Adapted from Fogler, 2005.*

Each of this mechanism will be analyzed in detail in the following sections.

1.1.1 Transport in the liquid film surrounding the particles

Referring to the reaction scheme of Fig. 1.1, the rate of external mass transfer $\dot{n}_A^{b\to i}$ of the liquid species A to the solid-liquid interface is defined as a product of the external mass transfer coefficient, $h_{m,A}$, the interfacial area for mass transfer per unit volume of liquid, $a^{L,i}$, and the concentration driving force, $(C_A^b - C_A^i)$:

$$\dot{n}_A^{b\to i} = h_{m,A}(C_A^b - C_A^i)a^{L,i}, \quad \left[mol_A/(m^3_{liquid}s)\right] \quad . \tag{1.1}$$

The variables C_A^b and C_A^i are the concentration of the liquid material in the bulk of the liquid and at the solid surface, respectively. The interfacial area for mass transfer per unit volume of liquid, $a^{L,i}$, is given by:

$$a^{L,i} = \frac{A^i}{V^L} \quad , \tag{1.2}$$

where A^i represents the external interfacial area between the solid and the liquid, excluding the area given by the porosity if the solid is porous, and V^L is the total liquid volume.

1.1.2 Pore-diffusion and surface reaction

If the reaction occurs between the liquid species A which reacts with the solid at the solid surface, the reaction rate per unit of area of the solid is indicated with R'' and its unit of measure is $mol/(m^2_{solid\ surf.}s)$. Its expression can vary dependently on the model chosen for the reaction rate and is usually a function of the concentration of the reactants at the solid surface or adjacent to it. R'' differs from the rate of formation (or consumption) of each species participating the reaction. For example, considering a species A which is consumed (or produced) during the reaction, its rate of consumption (or production) r''_A per unit area of solid surface is defined as the product of the reaction rate R'' and the stoichiometric coefficient of A in the reaction:

$$r''_A = \upsilon_A R'', \left[\frac{mol_A}{m^2_{solid\ surf.}s}\right] \quad . \tag{1.3}$$

Thus, the reaction rate of A per unit of liquid volume is usually conveniently expressed as the product of the reaction rate of A per unit area of solid evaluated at the external solid surface, $r''_A(C^i_A)$, the total surface area of the solid per unit volume of the liquid $a^{L,tot}$ and a term η to take into account the effect of the porosity in case of porous solids:

$$\dot{n}_A = r''_A \eta a^{L,tot}, \quad \left[mol_A/(m^3_{liquid}s)\right] \quad . \tag{1.4}$$

In this case the expression of $a^{L,tot}$ is:

$$a^{L,tot} = \frac{A^{tot}}{V^L} \quad , \tag{1.5}$$

where A^{tot} is the total surface area of the solid in contact with the liquid accessible to the reacting species, including the area given by the porosity, which is usually much greater than the external interfacial area A^i. If the solid is non-porous it results $A^{tot} = A^i$.
The term η is called *effectiveness factor* and is widely used to account for the interaction between pore diffusion and reactions on pore walls of the reacting fluid species in porous catalytic or reactive solid particles. The effectiveness factor is defined as the ratio of the reaction rate actually observed to the reaction rate calculated if the surface reactant concentration C^i_A persisted throughout the interior of the particle, that is, no reactant concentration gradient within the particle. The reaction rate in a particle can therefore be conveniently expressed by its rate under external surface conditions multiplied by the effectiveness factor, like in Eq. 1.4.

$$\eta = \frac{actual\ overall\ rate\ of\ reaction}{rate\ of\ reaction\ that\ would\ result\ if\ entire\ interior\ surface\ were\ exposed\ to\ the\ external\ pellet\ surface\ conditions\ C_A^i} = \frac{r_A''\ ,\ with\ diffusion}{r_A''\ ,\ without\ diffusion\ resistance} \tag{1.6}$$

The magnitude of the effectiveness factor (ranging from 0 to 1) indicates the relative importance of diffusion and reaction limitations.

The general expression of the effectiveness factor depends on the shape and dimension of the solid particles and the model used for the reaction rate R''. In some cases, instead of the reaction rate per unit area of solid R'', the reaction rate per unit volume of solid R''' is adopted. The relation between the two is:

$$R''' = R'' a^{S,tot}, \left[\frac{mol}{m^3_{solid^S}}\right] \ , \tag{1.7}$$

where $a^{S,tot}$, similarly to $a^{L,tot}$, is defined as the total surface area of the solid, A^{tot}, per unit volume of the solid particles, including the volume of the pores:

$$a^{S,tot} = \frac{A^{tot}}{V^{p,tot}} \ . \tag{1.8}$$

Using R''' the porous solid is considered like a unique pseudo-homogeneous phase, instead of a porous solid with fluid inside the pores.

Since in this work are used only spherical solid particles, the relative expression of η is:

$$\eta = \frac{1}{\phi}\left(\frac{1}{tanh(3\phi)} - \frac{1}{3\phi}\right) \ . \tag{1.9}$$

In the previous expression ϕ is called *Thiele modulus* and takes into account the effect of the particle dimensions toward the *particle characteristic length L*, the *effective diffusivity* of the liquid species in the porous particle $\mathfrak{D}_e$ and the reaction kinetics R'''. Its expression for first order monomolecular and *n*th order monomolecular reactions is (Levenspiel, 1999):

$$\phi = L\sqrt{\frac{k'''}{\mathfrak{D}_e}}, \quad R''' = k''' C_A^i \tag{1.10}$$

$$\phi = L\sqrt{\frac{(n+1)k''' {C_A^i}^{n-1}}{2\mathfrak{D}_e}}, \quad R''' = k''' {C_A^i}^n \tag{1.11}$$

The characteristic length of the particle L is generally defined as:

$$L = \frac{volume\ of\ the\ particle}{\substack{exterior\ surface\ available \\ for\ reactant\ penetration}} \quad . \tag{1.12}$$

For spherical particles of diameter d_p it becomes:

$$L = \frac{d_p}{6} \quad . \tag{1.13}$$

The effective diffusivity account for the fact that:

- not all of the area normal to the direction of the flux is available (i.e. the area occupied by solids) for the molecules to diffuse;
- the paths are tortuous.

An equation that relates $\mathfrak{D}_e$ to the liquid bulk diffusivity $\mathfrak{D}_{A,L}$ is:

$$\mathfrak{D}_e = \frac{\mathfrak{D}_{A,L}\varepsilon_p}{\tau} \quad , \tag{1.14}$$

where ε_p is the porosity of the solid particle and τ is defined as the tortuosity of the pores. It describes the difference of the catalyst pores from the ideal linear, cylindrical form. Particle porosity is always smaller than one, whereas tortuosity is larger than one.

The theoretical determination of tortuosity is model dependent and extremely cumbersome for all but the most simple geometries. It is most often the case that $\mathfrak{D}_e$, $\mathfrak{D}_{A,L}$ and ε_p in equation (1.14) are determined experimentally and τ is then calculated from these.

Typical values of the tortuosity and the pellet porosity are, respectively, 3 and 0.4 (Fogler, 2005).

A plot of the effectiveness factor as a function of the Thiele modulus is shown in Figure 1.4.

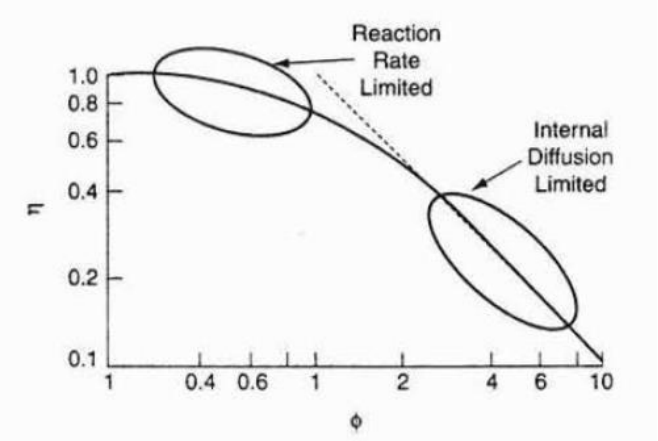

Figure 1.4. *Plot of η as function of the Thiele modulus ϕ. Adapted from Fogler, 2005.*

As the particle diameter becomes very small, ϕ decreases, so that the effectiveness factor approaches 1 and the reaction is surface-reaction-limited. On the other hand, when the Thiele modulus ϕ is large, the internal effectiveness factor η is small (i.e. $\eta \ll 1$) and the reaction is diffusion-limited within the pellet. In this last case the expression of the effectiveness factor becomes:

$$\eta = \frac{1}{\phi} \quad , \tag{1.15}$$

and the curve depicted in Fig. 1.4 becomes linear.

1.2 Determining the controlling regime

A key issue in solid-liquid reactions is the determination of the controlling process regime: mass transfer in the liquid film surrounding the solid particles, internal mass transfer due to the diffusion of the liquid species into the pores or chemical reaction occurring at the solid surface. Experimentally, this is done by checking the effect of some parameters on the observed process rate. A common parameter which can give very useful information about the controlling regime is the reaction temperature, however the effect of it is not examined here because it wasn't used for the study object of this thesis.

It is fundamental to know the regime of a particular reaction system, since the equipment choice and the effect of design and operating variables on the process performance depend on the regime.

However is important to remember that is not always possible to identify a controlling step, intermediate conditions between regimes are also possible when the magnitude of the different mechanisms is similar.

1.2.1 Identifying external mass transfer limitations

Solid-liquid mixing operations involving chemical reactions often require a high relative velocity between the solid particle and the liquid (high local shear rate or agitation intensity) to minimize the thickness of the boundary layer for mass transfer (Paul, Atiemo-Obeng & Kresta, 2004).

Most solid-liquid mixing operations operate above the minimum speed for suspension. A higher agitation speed improves the degree of suspension and enhances mass transfer rates. The higher speed also translates into higher turbulence as well as local and average shear rates.

The properties of both the liquid and the solid particles influence the fluid-particle hydrodynamics and thus the suspension and the mass transfer. Also important are vessel geometry and agitation parameters.

If the external mass transfer is the rate determining step the concentration of the liquid reacting species, for example A, at the external interface of the solid, C_A^i, is null because they are consumed very quickly by the solid and the overall reaction rate of A per unit volume of the liquid $(r_A)_{obs}$ reduces to equation (1.1):

$$(r_A)_{obs} = \dot{n}_A^{b\to i} = h_{m,A} C_A^b a^{L,i}, \left[\frac{mol_A}{m^3_{liquid} s}\right] \quad , \tag{1.16}$$

The external mass transfer rate is affected primarily by the impact of agitation on the hydrodynamic environment near the surface of the particle. The hydrodynamic environment near the particle surface depends on the properties of the fluid as well as those of the particles. The important hydrodynamic variables are the relative velocity, v_s, between the solids and the liquid (also know as slip velocity) and the rate of renewal of the liquid layer near the solid surface. The relative velocity, v_s, obviously varies from point to point within the vessel, and the average value is difficult to estimate.

The observed effect of agitation is depicted in Figure 1.5. As the stirrer speed (proportional to the power per unit volume of liquid transferred to the liquid) increases, the volumetric mass transfer coefficient, $h_{m,A}a^{L,i}$, increases. If the process is mass transfer controlled, the observed rate of reaction increases with increasing impeller speed.

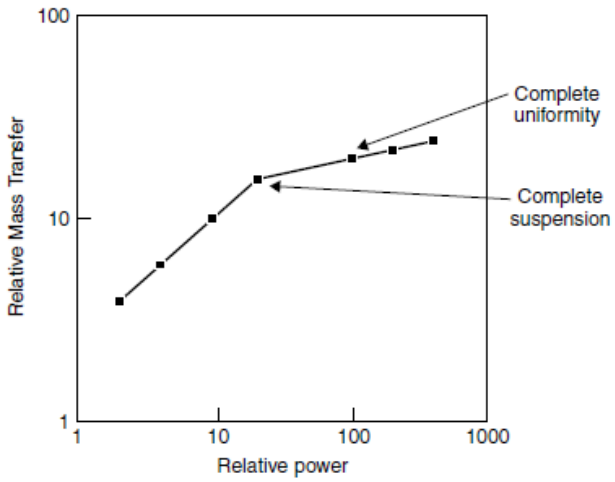

Figure 1.5. *Relative external mass transfer trend as function of the relative power given to the liquid (proportional to the stirring rate). Adapted from Paul, Atiemo-Obeng & Kresta, 2004.*

However, beyond the just suspended or complete suspension state the observed rate may not increase much with increasing rpm or mixing intensity. For extremely slow reactions on-bottom motion to prevent stagnant pockets may be all that is needed.

1.2.2 Identifying internal mass transfer limitations

For systems in which the diffusion of the liquid species inside the pores is the limiting regime, the observed overall reaction rate corresponds to equation (1.4) with the asymptotic value of η of equation (1.15):

$$(r_A)_{obs} = \dot{n}_A = r_A'' \frac{1}{\phi} a^{L,tot} \quad . \tag{1.17}$$

The presence (or absence) of pore-diffusion resistance in catalyst particles can be readily determined by evaluation of the Thiele modulus and subsequently the effectiveness factor, if the intrinsic kinetics of the surface reaction are known.
When reactant fully penetrates the particle and bathes all its surfaces, then the particle is in the diffusion free regime. This occurs when MT < 0.4 (Levenspiel, 1999).
At the other extreme when the center of the particle is starved for reactant and is unused then the particle is in the strong pore resistance regime. This occurs when MT > 4.
This is shown in Figure 1.6.

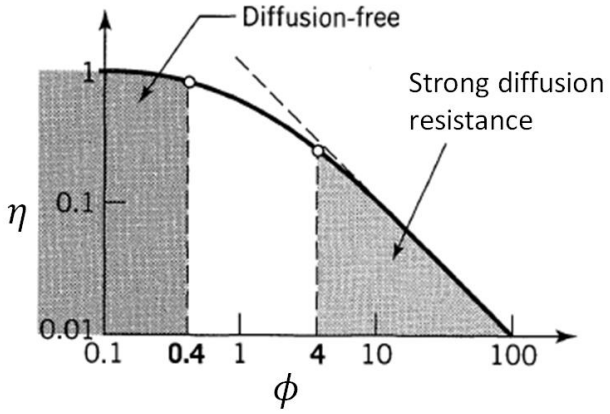

Figure 1.6. *Limits for negligible and for strong pore diffusion resistance.*

When the intrinsic rate law is not known completely, so that the Thiele modulus cannot be calculated, there are other methods available. One of these is based upon measurement of the rate for differing particle sizes (Missen, Mims and Saville, 1999) and does not require any knowledge of the kinetics.
If the rate of reaction, $(r_A)_{obs}$, is measured for two or more particle sizes (values of characteristic length L), two extremes of behaviour may be observed:

- the rate is independent of particle size. This is an indication of negligible pore-diffusion resistance, as might be expected for either very porous particles or sufficiently small particles such that the diffusional path-length is very small. In either case, $\eta \rightarrow 1$, and $(r_A)_{obs} = r_A''(C_A^i)a^{L,tot}$ for the surface reaction;

- the rate is inversely proportional to particle size. This is an indication of strong pore-diffusion resistance, in which $\eta \to 1/\phi$ as $\phi \to large$. Since $\phi \propto L$, for fixed other conditions (surface kinetics, $\mathfrak{D}_e$, and C_A^i), if measured rates for two particle sizes (denoted by subscripts 1 and 2) are compared for strong pore-diffusion resistance:

$$\frac{(r_A)_{obs,1}}{(r_A)_{obs,2}} = \frac{\eta_1}{\eta_2} = \frac{\phi_2}{\phi_1} = \frac{L_2}{L_1} = \frac{d_{p,2}}{d_{p,1}} \quad . \tag{1.18}$$

1.2.3 Identifying surface kinetics limitations

When the slow processes are not the external or internal mass transfer anymore, the overall reaction rate could be controlled by the kinetics of the surface reaction. If this is the case, the parameters that affect the external and internal mass transfer, i.e. the agitation speed and the solid particles diameter, don't have any effect on the observed reaction rate which corresponds to the reaction rate of the surface reaction with $\eta = 1$:

$$(r_A)_{obs} = r_A'' a^{L,tot} \quad . \tag{1.19}$$

Chapter 2

The SpinChem® Rotating Bed Reactor

In this chapter is described the reactor that have been studied in this work: the SpinChem® rotating bed reactor (abbreviated RBR). This new type of reactor is made for heterogeneous reactions, in particular solid-liquid reactions, where the solid can be a catalyst or a reactant itself. It can also have applications in reactions involving two liquid phases, but this hasn't been studied in this work.

The RBR constitutes an alternative to the common two-phase solid-liquid reactors like the stirred tank reactor (STR) or packed bed reactor (PBR).

In this work the performance of the RBR have been investigated and compared with a normal stirred tank reactor using two different solid-liquid reactions, whose general aspects are described in Chapter 1.

2.1 The reactor and its working principle

The SpinChem® rotating bed reactor is a reactor made for heterogeneous reactions, especially solid-liquid reactions. The entire reactor is shown in Figure 2.1.

Figure 2.1. *A SpinChem® RBR S311 placed in a 1200 mL vessel (on the left) and a SpinChem® RBR S221 in a 210 mL vessel (on the right).*

It consists in two main parts: an external vessel and an internal stirring element, the rotating bed.

The choice of the vessel is up to the user but is worthwhile to remember that its geometry and the type of baffles used can affect the hydrodynamic of the system and consequently the performances of the reactor. SpinChem AB provides glass jacketed vessels with *flower-baffles*. Flower-baffles are particular type of baffles consisting in many (eighteen) tiny baffles engraved directly on the internal wall of the vessel, a view of them from the top of the vessel is shown in Figure 2.2.

Figure 2.2. *The interior of a flower-baffled vessel with eighteen baffles from the top.*

The most important and innovative part of the reactor is the stirring element, depicted in Figure 2.3.

It consists of a cylindrical cavity with a drive shaft attached to the top cover, a central inlet in the bottom, and a multitude of screened outlets on the peripheral cylindrical surface.

On the internal side of the perforated wall there is a metallic cylindrical outer filter which ensures that the solid particles stay inside the basket. A cylindrical inner filter with the same function and a smaller diameter is present around the central part of the basket, as shown in Fig. 2.3 d) and e).

The open basket of Fig. 2.1 c) and d) is then closed with an annular top lid which is kept tight by screwing the upper piece (air outlet) with two tiny holes visible in Fig. 2.1 a) and e). To this piece is then connected the shaft.

The RBR holds the solid phase as a packed bed and when the unit is rotated in a liquid, centrifugal force conveys liquid from the central inlet, through the solid that fills the internal cavity, and discharges it through the peripheral outlets, as shown in Figure 2.4. When operated, the rotary action creates a toroidal liquid flow below the unit flow in the liquid medium being processed, which leads to the creation of a vortex towards the inlet at the bottom. The unit thus sucks liquid also from the depth of the liquid volume and discharges it in a radial manner at the surface.

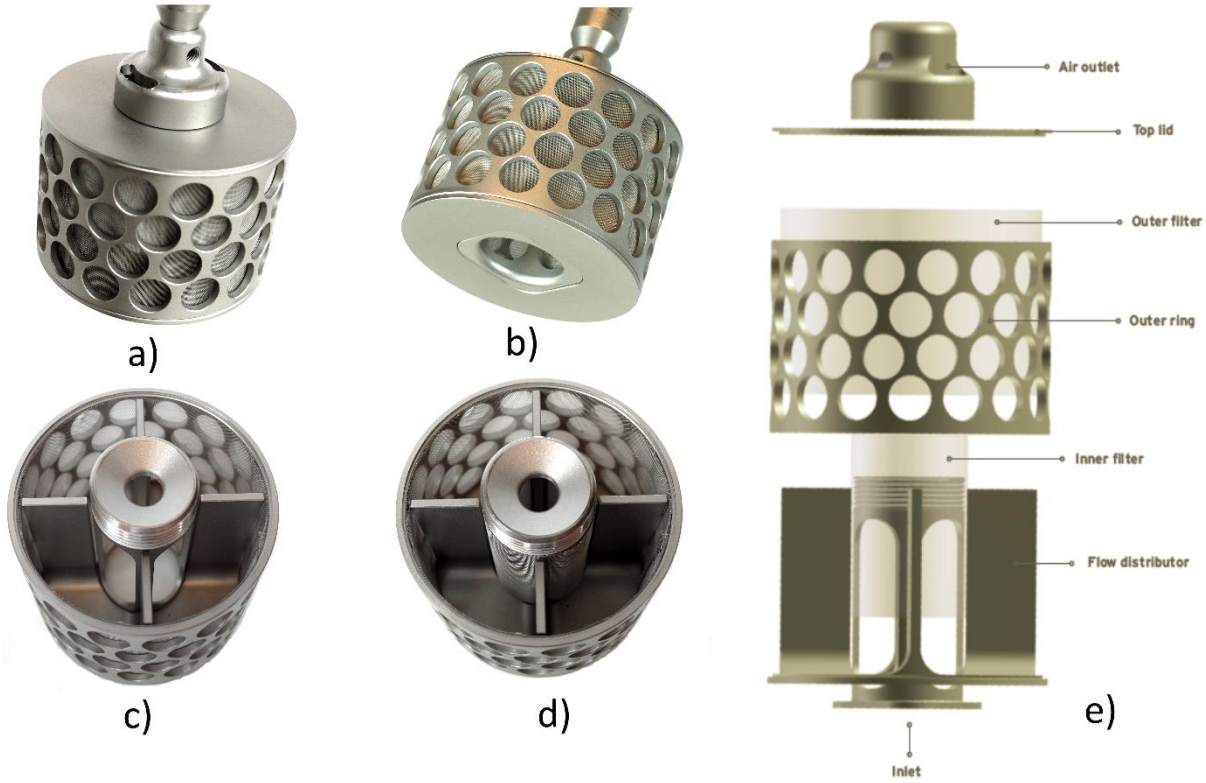

Figure 2.3. *The SpinChem® RBR S221.*

If necessary, the stirring element can initially draw a suspended solid from the liquid into the treatment chambers, where the material then stays during the processing and allows facile recovery.

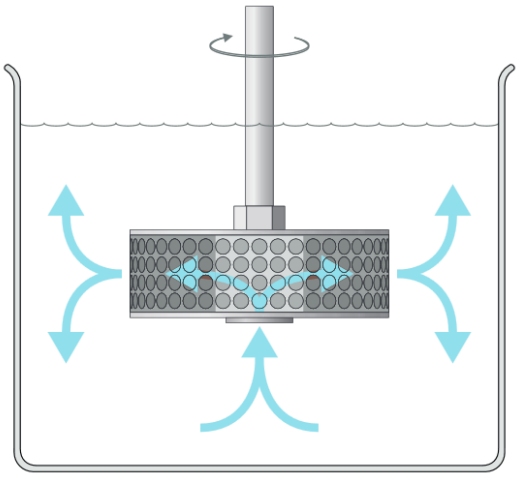

Figure 2.4. *Flow patterns in the SpinChem® rotating bed reactor.*

2.2 Solid-liquid external mass transfer in the rotating bed reactor

As reported in the paragraph §1.2.1 of Chapter 1, the mass transfer in the external film surrounding the solid particles in solid liquid reactions is influenced by the relative velocity (or slip velocity), v_s, between the solid and the liquid and the rate of renewal of the liquid layer near the solid surface.

In slurry reactors (STR) the dispersed solid particles move together with the surrounding liquid, resulting in a slow relative velocity between the two phases.

The idea behind the RBR is to enhance the external mass transfer by increasing the slip velocity v_s. In the RBR the solid particles are immobilized inside the cylinder and the liquid is forced through the bed by the centrifugal force.

The rotational speed - plus other factors such as bed permeability - will affect the flow rate through the RBR.

Chapter 3

Scavenging of genotoxic impurities

In this chapter the performances of the RBR are studied and compared with those of a slurry reactor stirred by a common axial impeller. We used a solid-liquid reaction to remove, or scavenge, an undesirable impurity from a liquid solution by means of a solid sorbent. The solid selected is made of small spherical particles that can be placed in the RB or directly in the vessel (dispersed) if a normal impeller is used instead.
Prior to the investigation of the reactor performances, it was also necessary to study and understand the reaction itself, since not too many previous studies on this type o reaction were found.
In the chapter are also reported the theoretical backgrounds on the reaction, the set-up of the analytical method and how the final reaction conditions (solvent, catalyst, temperature etc.) were chosen.

3.1 Theoretical aspects

The reaction selected to test the RBR is of industrial importance because it helps the removal of harmful impurities from pharmaceutical products. In this paragraph the reaction is presented first, from the industrial and legislative point of view and, after that, from the chemical point of view.

3.1.1 The problem of genotoxic impurities in the pharmaceutical industry

The synthesis of pharmaceutical products frequently involves the use of reactive reagents and the formation of intermediates and byproducts.
Low levels of some of these may be present in the final drug substance and drug product as impurities (Müller et al., 2006). Such chemically reactive impurities may have at the same time the potential for unwanted toxicities including genotoxicity and carcinogenicity and hence can have an impact on product risk assessment.
Genotoxic compounds induce genetic mutations and/or chromosomal rearrangements and can therefore act as carcinogenic compounds. These compounds cause damage to DNA by different mechanisms such as alkylation or other interactions that can lead to mutation of the genetic codes.

Genotoxicity pertains to all types of DNA damage (effects from mutagenicity through DNA reactivity, DNA damage, and chromosomal damage, both structural chromosome breakage and aneuploidy), whereas mutagenicity pertains specifically to mutation induction at the gene and chromosome levels (Jouyban and Pars, 2012).

The pharmaceutical industry and those that regulate it recognize their respective obligation to limit genotoxic impurities. Therefore, substantial efforts are made during development to control all impurities at safe concentrations.

The United States Food and Drug Administration (FDA), and equivalent international healthcare agencies, require that harmful impurities in drug products be controlled and removed to below regulated limits. Genotoxins are a challenging class of impurities that have proven to be harmful even at low concentrations and as a result regulatory bodies have specifically defined their limits in drug substances and products (Agilent Technologies (2013)).

Müller et al., 2006 proposed that impurities be classified into one of five classes using data (published in the literature or from genotoxicity testing) and comparative structural analysis to identify chemical functional moieties correlated with mutagenicity.

The five classes are:

- Class 1 – Impurities known to be both genotoxic (mutagenic) and carcinogenic;
- Class 2 – Impurities known to be genotoxic (mutagenic), but with unknown carcinogenic potential;
- Class 3 – Alerting structure, unrelated to the structure of the API (active pharmaceutical ingredients) and of unknown genotoxic (mutagenic) potential;
- Class 4 – Alerting structure, related to the API;
- Class 5 – No alerting structure or sufficient evidence for absence of genotoxicity.

Some widely recognized alerts for DNA reactivity, i.e., mutagenic activity, are depicted in Figure 3.1.

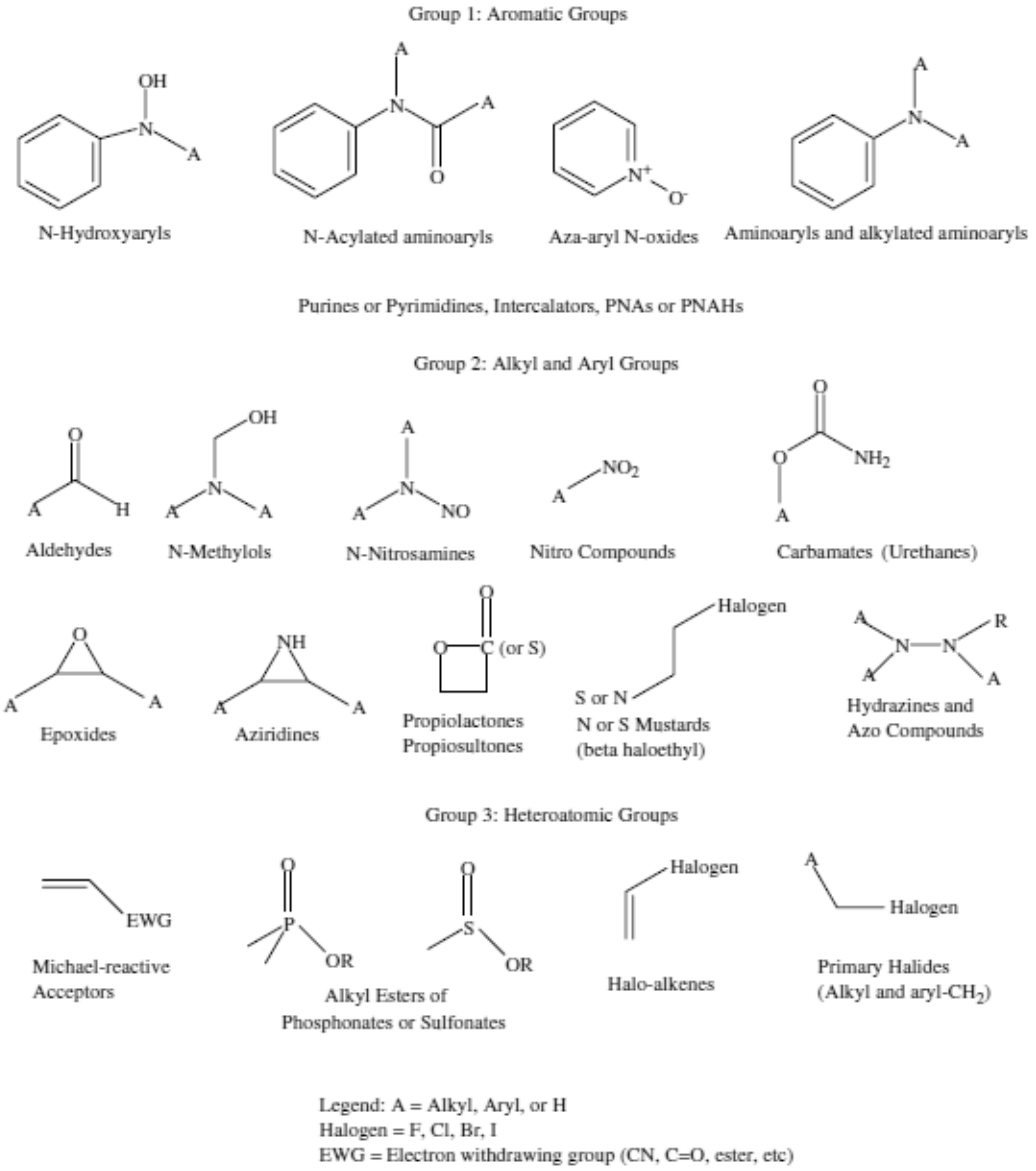

Figure 3.1. *Some examples of structurally alerting functional groups that are known to be involved in reactions with DNA (Müller et al., 2006).*

For drug substance, the identification thresholds are within the range of 500 and 1000 ppm (i.e., 0.05 and 0.1%). ICH Guidelines Q3A(R) and Q3B(R) state that although identification of impurities is not generally necessary at levels less than or equal to the identification threshold, ‘‘analytical procedures should be developed for those potential impurities that are expected to be unusually potent, producing toxic or pharmacological effects at a level not more than the identification threshold.’’ Thus in the case of impurities where a potential safety concern for genotoxicity exists, the guidelines imply that the routine identification threshold is not considered to be applicable.

To address this problem in a general way valid for every genotoxic impurity, in absence of adequate toxicity data allowing a compound-specific risk assessment, is now proposed a general

concept that is based on the knowledge and approaches as defined by the Threshold of Toxicological Concern (TTC). In agreement with the CHMP Draft Guideline on Genotoxic the TTC concept is used to establish a limit of 1.5 μg/day, corresponding to a 10^{-5} lifetime risk of cancer, as a virtually safe dose for most genotoxic compounds, while recognizing that some highly potent genotoxic compounds may require even lower levels.
The concentration limits in ppm of genotoxic impurity in drug substance derived from the TTC can be calculated based on the expected daily dose to the patient using equation (3.1):

$$Concentration\ limit\ [ppm] = \frac{TTC\ [\mu g/day]}{dose\ [g/day]} \quad . \tag{3.1}$$

A TTC value higher than 1.5 μg/day may be acceptable under certain conditions, e.g. short-term exposure.
Considering the strictest acceptable daily intake (ADI) of 1.5 μg/day, the concentration limits corresponding to various values of daily dose are reported in Table 3.1.

Table 3.1. *Relationship between acceptable daily intake (ADI) levels and daily dose of a pharmaceutical (active pharmaceutical ingredient, API) for daily doses between 1 and 3000 mg*

Daily dose of API [mg]	ADI [μg/day]	Concentration limit [ppm]
3000	1.5	0.5
1000	1.5	1.5
500	1.5	3
100	1.5	15
50	1.5	30
25	1.5	60
10	1.5	150
5	1.5	300
1	1.5	1500

From Table 3.1 is clear that the lowest concentration limits correspond to some ppm levels, depending on the daily dose. Hence is necessary, in the worst case, to control the concentration of the impurity below these levels. If the genotoxic impurity in the desired product is in greater concentration is necessary to find a clean and safe way to remove it.

3.1.2 Selected genotoxic impurity and solid scavenger

The idea that has been studied in this work is to use a solid reactant, called scavenger, that is able to react with the genotoxic impurity and link it on its surface. This method applies only to the purification of liquid products. At the end the exhaust solid can be removed from the

purified solution by filtration. This process can be carried out either in a normal STR or in the RBR.

To try this idea, a genotoxic impurity was selected, in the class of the Michael-reactive acceptors (see Figure 3.1). Michael acceptors can undergo cytotoxic reactions with nucleophilic cellular constituents. Of particular concern are potentially genotoxic reactions of Michael acceptors with nucleic acid nucleophiles (Balu et al., 2004).

A real example in which such type of impurity is produced is the synthesis of the active pharmaceutical ingredient (API) oxycodone, an analgesic generally indicated for relief of moderate to severe pain.

Oxycodone is a semisynthetic opiate produced via an oxidative conversion of the natural product thebaine to l4-hydroxycodeinone as depicted in the scheme of Figure 3.2.

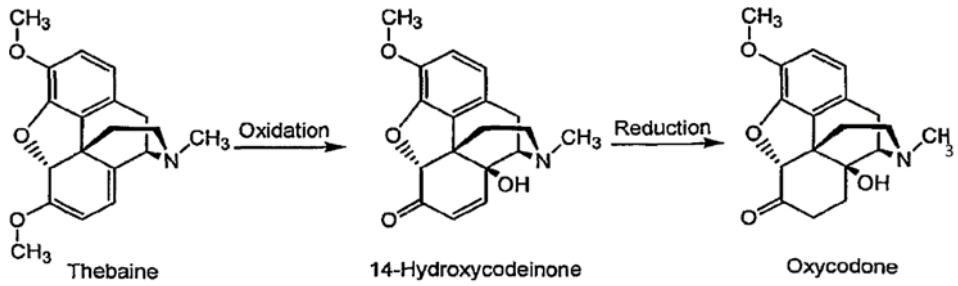

Figure 3.2. *Oxycodone production steps*

The oxycodone precursor l4-hydroxycodeinone is a Michael acceptor that commonly contaminates oxycodone preparations. These two compounds are very similar and the only difference is the presence of a carbon-carbon double bond conjugated with the double bound of the carbonyl group in the l4-hydroxycodeinone.

Some ways to remove 14-hydroxycodeinone impurities from oxycodone in different reaction conditions have already been proposed. One of these includes the use of a solid reactant (scavenger) made of an inert support functionalized with thiol groups (Controlled Chemicals, Inc., Colmar, PA (US), 2015).

To try the reaction, simpler and more common compounds were used instead of the couple oxycodone – 14-hydroxycodeinone. These compounds are the cyclohexanone, representative of the oxycodone, and the 2-cyclohexen-1-one (or cyclohexenone), analogous of the l4-hydroxycodeinone. The compounds and the analogy are shown in Figure 3.3.

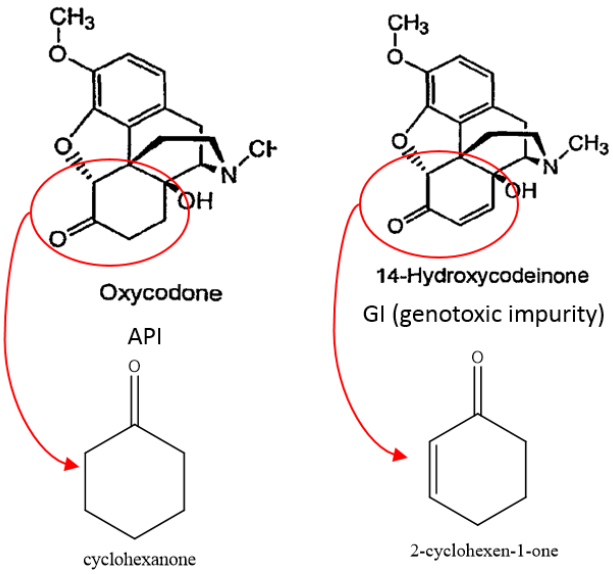

Figure 3.3. *Real API-GI system (oxycodone – 14-hydroxycodeinone) and simplified API-GI system (cyclohexanone – 2-cyclohexen-1-one) chosen for the study.*

14-hydroxycodeinone and 2-cyclohexen-1-one belong to the class of the α,β-unsaturated carbonyl compounds, with the general structure of Figure 3.4.

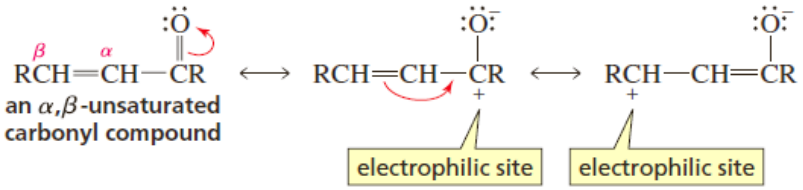

Figure 3.4. *General structure of α,β-unsaturated carbonyl compounds (Bruice, 2004).*

α,β-unsaturated carbonyl compounds are often attacked by nucleophiles at the β carbon.
The idea was to use a solid state nucleophile to remove the traces of 2-cyclohexen-1-one from the solution of 2-cyclohexen-1-one and cyclohexanone. The selected solid nucleophile (scavenger) is made of porous spheres of inert fused silica gel functionalized with thiol groups (TG), that are the nucleophilic sites (see §3.2.1). The expected reaction is represented in Figure 3.5.

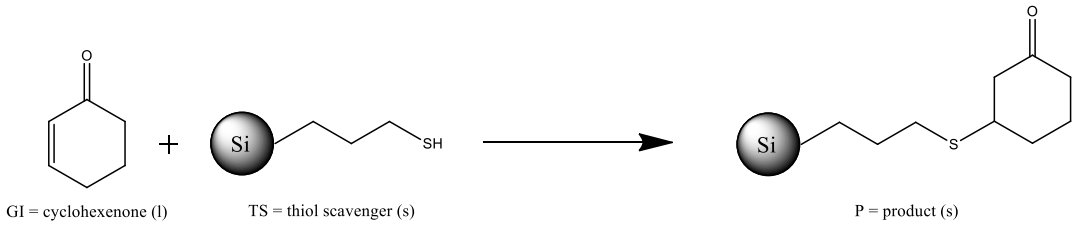

Figure 3.5. *Expected reaction of the 2-cyclohexen-1-one with the thiol scavenger.*

The product formed is a solid called thioether. As mentioned at the end of §3.1.1 the target, as required by the guidelines, is to reach a final GI concentration of 10 ppm or lower, corresponding to the lowest concentrations allowed.

3.1.3 Nucleophilic conjugate addition to α,β-unsaturated carbonyl compounds

As shown in Figure 3.4, α,β-unsaturated carbonyl compounds contain two electrophilic sites: the carbonyl carbon and the carbon atom that is β to it. This means that a nucleophile can add either to the carbonyl carbon or to the β-carbon.
Nucleophilic addition to the carbonyl carbon is called direct addition or 1,2-addition.

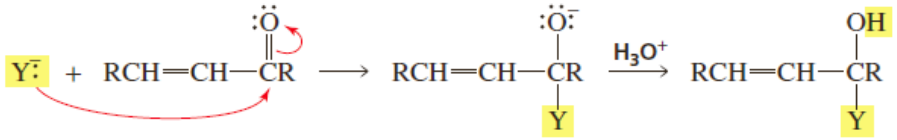

Figure 3.6. *1,2-addition or direct addition mechanism (Bruice, 2004).*

With certain nucleophiles, addition takes place at the carbon-carbon double bond rather than at the carbonyl group, this is called 1,4-addition or conjugate addition. After 1,4-addition has occurred, the product, an enol, tautomerizes to a ketone, so the overall reaction amounts to addition to the carbon-carbon double bond, with the nucleophile and a final protonation by a proton from the reaction mixture adding to the α-carbon.

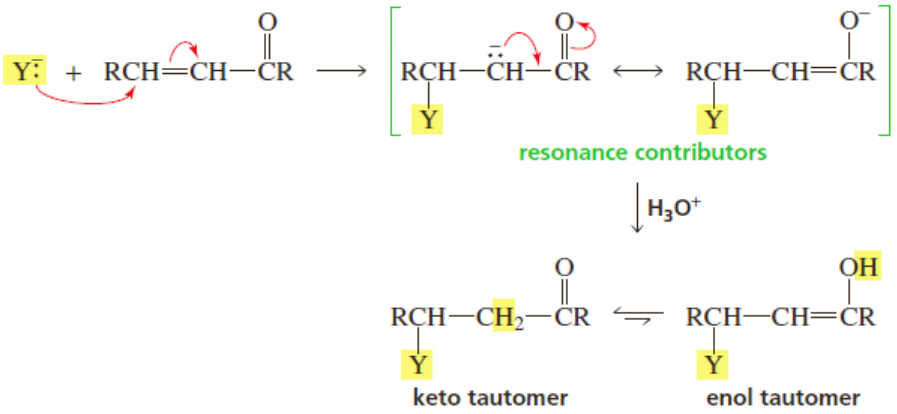

Figure 3.7. *1,4-addition or conjugate addition mechanism (Bruice, 2004).*

Whether the product obtained from nucleophilic addition to an α,β-unsaturated aldehyde or ketone is the direct addition product or the conjugate addition product depends on the nature of the nucleophile, the structure of the carbonyl compound, and the conditions under which the reaction is carried out.

Nucleophiles that form unstable addition products - that is, nucleophiles that are weak bases, allowing direct addition to be reversible - form conjugate addition products because they are more stable. Nucleophiles in this group include halide ions, cyanide ion, thiols, alcohols, and amines (Bruice, 2004).

Homogeneous reactions between α,β-unsaturated carbonyl compounds and liquid thiols have already been reported by Krishnaveni et al., 2005, Movassagh and Shygan, 2006, Khatik *et al.* (2006), Controlled Chemicals, Inc., Colmar, PA (US), 2015.

Also aldehydes and ketones, like cyclohexanone and oxycodone, react with thiols to form thioacetals and thioketals. However a thiol is a poor nucleophile and an acid catalyst is required for the reaction to take place at a reasonable rate (Bruice, 2004). Provided this, the API (cyclohexanone) shouldn't react with the thiol scavenger but is better to check it in the practice.

In the case of thiols, the nucleophilic species able to attack the double bond of the GI is the sulfur anion or thiolate anion. For that reason the thiol groups must undergo a deprotonation before reacting. The overall reaction mechanism is depicted in Figure 3.8.

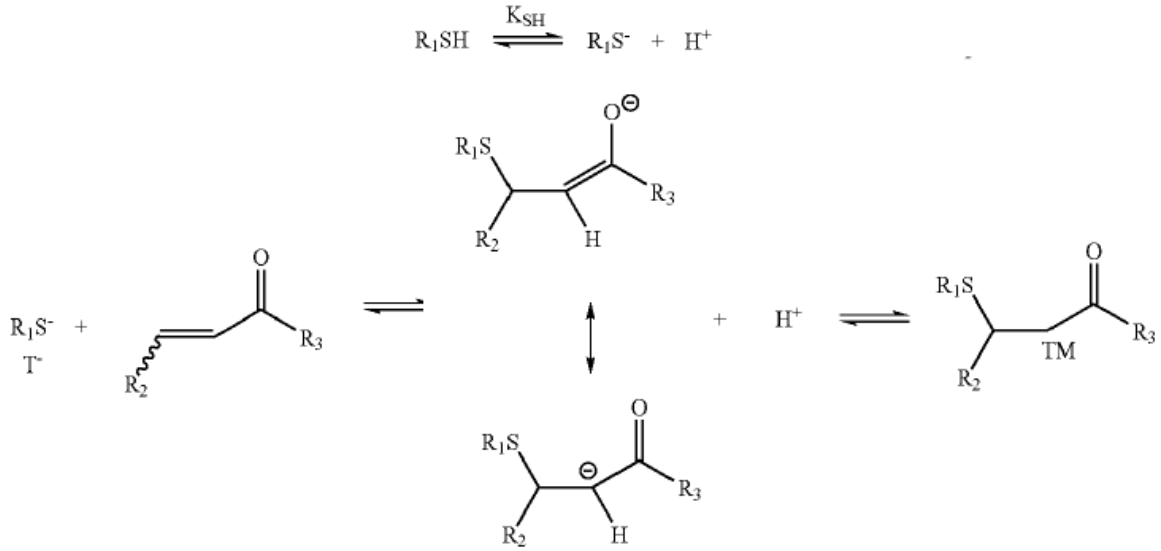

Figure 3.8. *Mechanism of the thiol conjugate addition to α,β-unsaturated carbonyl compounds.*

According to Controlled Chemicals, Inc., Colmar, PA (US), 2015 and Müller et al., 2006, the rate determining step in these types of reactions is the formation of the charged intermediate. The deprotonation of the thiol and the final proton transfer should be fast reactions.

The deprotonation of the thiol is an equilibrium reaction and is affected by the nature (acidity) of the thiol and the pH of the environment. Schmidt et al., 1999 and Shi and Greaney, 2005 reported that the reactivity of the thiol compounds, thus the overall reaction rate, increases with the pH due to the formation of the thiolate anion. Mather et al., 2006, Sarathi *et al*., 2008 and Li et al., 2010 refer to the use of a suitable basic catalyst to increase the reaction rate. The base is used to promote the deprotonation of the nucleophile, in this case the thiol.

An example of a suitable base that have been used with thiols by Sarathi *et al*., 2008 and Li *et al*., 2010 is triethylamine.

This base is a moderate basic non-nucleophilic base. A non-nucleophilic base is an organic base that is a poor nucleophile. Normal bases are also nucleophles, but often chemists seek the proton-removing ability of a base without any other functions. Typical non-nucleophilic bases are bulky, such that protons can attach to the basic center but alkylation and complexation is inhibited (Wikipedia, 2015). Some examples of these bases are: N,N-diisopropylethylamine (DIEA), triethylamine (TEA), 1,8-diazabicycloundec-7-ene (DBU), 2,6-di-tert-butylpyridine and phosphazene bases. They are reported in Figure 3.9.

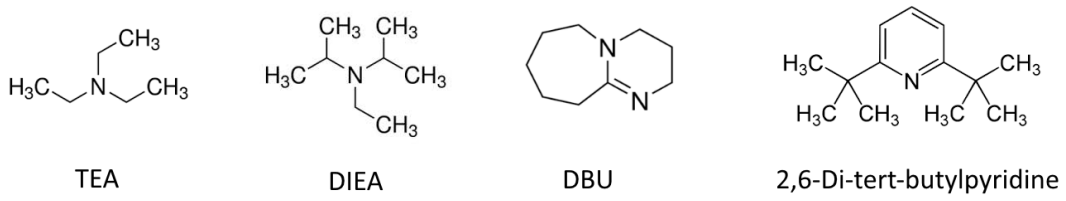

Figure 3.9. *Some examples of non-nuchleophilic bases commonly employed in organic chemistry.*

As reported by Mather *et al*., 2006, solvent plays an important role when carbon nucleophiles are used. Typical solvents for the carbon-Michael reaction include methanol, ethanol, diethyl ether, tetrahydrofuran, benzene, xylene, dioxane and mixtures of these solvents. Protic solvents seem to be desirable in the carbon-Michael reaction to promote rapid proton transfer and to stabilize charged intermediates.

Barahman and Pershang, 2006 have reported also the addition of thiols to α,β-unsaturated carbonyl compounds under solvent-free conditions.

3.2 Instruments, materials and methods

In this section all the information regarding the experimental part are reported: the substances used, the laboratory equipment, the analytical instruments and the experimental design and methods.

3.2.1 Substances

The substances used, divided by type, and the respective relevant properties are reported in Table 3.2.

Table 3.2. *List of the substances used and their main properties*

Substance	Function	Aggregation state at room temperature	Boiling point [° C]
2-cyclohexen-1-one	reactant	liquid	171-173
Thiol scavenger	reactant	solid	-
Cyclohexanone	product to purify (solvent)	liquid	155
N,N-diisopropylethylamine	catalyst	liquid	126
Ethanol	solvent	liquid	78
Methanol	solvent	liquid	64
Dimethylformamide	solvent	liquid	152-154
Tetrahydrofuran	solvent	liquid	66
Dichloromethane	solvent	liquid	39
n-octane	solvent	liquid	125

The thiol scavenger (TS) used is the SiliaMetS® Thiol by SiliCycle, commonly used for the scavenging of metals. It is made of spherical particle of fused silica functionalised with propane-thiol groups (TG) and was available in three different particle sizes. The characteristics of the three scavengers are listed in table 3.3.

Table 3.3. *Characteristics of the three scavengers used.*

Diameter (d_p) [µm]	Capacity [$mmol_{TG}/g$]	Specific surface area (S_a) [m^2/g]	Specific pore volume (spv) [mL/g]	Pore diameter [Å]
40-63	1.27	480-500	0.70-0.85	55-65
120-200	1.44	481	0.72	55-65
200-500	1.22	509	0.82	55-65

The aspect of the thiol scavenger is reported in Figure 3.9.

Figure 3.10. *A picture of the thiol scavenger SiliaMetS® Thiol from SiliCycle used (particle size = 200-500 μm).*

3.2.2 Reactors

Three types of reactor have been used:

1. the glass flask with magnetic stirring;
2. the SpinChem® RBR S221
3. a conventional stirred tank reactor (STR).

The glass flasks (25 mL) are used for the screening trials and the optimization of the reaction conditions. For the reactions carried out at high temperature they are combined with an oil bath heated by the hot plate, a thermocouple to measure and keep the desired temperature and, if needed, a laboratory glass condenser cooled with water. They are shown in Figure 3.11.

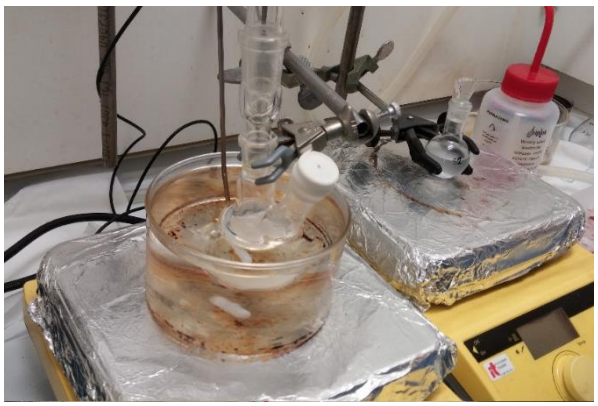

Figure 3.11. *The glass flasks used for the study of the reaction. The one on the left is placed in an oil bath and connected with a condenser.*

The RBR and the STR used are represented in Figure 3.12.

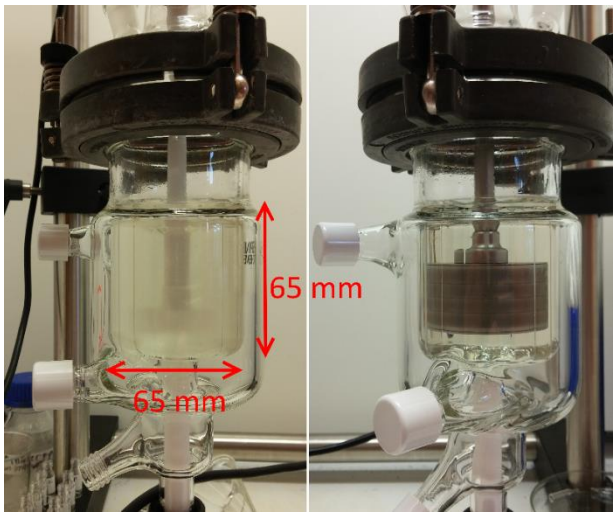

Figure 3.12. *The STR and the RBR S221.*

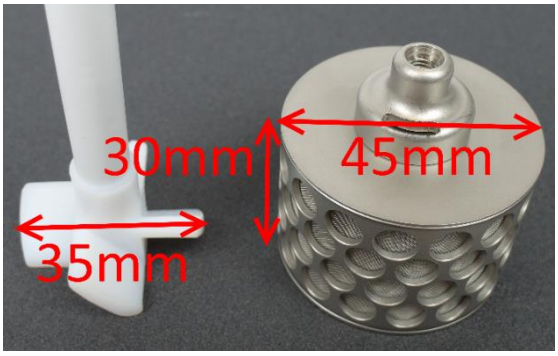

Figure 3.13. *Stirring elements used in the RBR and in the STR.*

Table 3.4. *Properties of the vessel, the rotating bed and the impeller used.*

Vessel	Rotating bed	Impeller
volume: V = 210 mL height: H_V = 65 mm diameter: D_V = 65 mm flower-baffled (18 flower baffles), see Fig. 2.2	volume: V_{RB} = 28 mL width: W_{RB} = 30 mm diameter: D_{RB} = 45 mm	type: pitched-blade # of blades: 4 diameter: D_I = 35 mm width of the blades: W_I = 12 mm;

The difference between the two is only in the stirring element; that is a rotating bed in the first case and a Teflon, 4-blades pitched-blade impeller for the STR. The latter is an axial mixer, that rotates to force a downdraft circulation. They are shown in Fig. 3.13.
The properties of the vessel and the stirring elements are listed in Table 3.4.

3.2.3 Analytical method

Since the TS and the product of the reaction in Figure 3.5 are solids, the best way to obtain the conversion of the 2-cyclohexen-1-one is to analyse its concentration.

Since all the species used in the system, except the scavenger, were liquid with relatively low boiling points (see Table 3.2), the concentration of the GI was obtained with the gas cromatograph (GC) and a flame-ionization detector (FID).
The GC used (Figure 3.14) is an Agilent 7820A with automatic sampler and the column a Restek Rtx®-50-DHA capillary column (maximum column temperature = 340° C).

Figure 3.14. *The GC-FID Agilent 7820A with auto-sampler used for the analysis of the concentrations.*

Two set-up of the GC parameters were used. The initial set-up (Set-up 1) was used at the beginning, than it was changed to another set-up (Set-up 2) to obtain shorter analysis time and higher detection limit. All the parameters of the two set-up are reported in Table 3.5.

Table 3.5. *Characteristics of the two set-up of the GC used.*

Parameter	Set-up 1	Set-up 2
Injection volume [μL]	0.2	0.2
Solvent A washes preinj.	0	0
Solvent A washes postinj.	5	5
Solvent B washes preinj.	0	0
Solvent B washes postinj.	5	5
Sample washes	5	5
Sample pumps	4	4
Inlet heater temperature [° C]	250	250
Inlet pressure [psi]	21.3	21.3
Carrier gas	nitrogen	nitrogen
Mode	split	split
Split ratio	100:1	10:1
Initial oven temperature [° C] / holding time [min]	80 / 0	80 / 0
Ramp 1 [°C/min]	10	5
Oven final temperature 1 [°C] / holding time [min]	280 / 0	130 / 0
Ramp 2 [°C/min]	-	30
Oven final temperature 2 [°C] / holding time [min]	-	300 / 0
FID detector temperature [° C]	250	250

Since the reaction mixture is made of cyclohexanone and 2-cyclohexen-1-one, first the separation of these two compounds was attempted, in a roughly 1:1 volume mixture using the GC set-up 1. The composition of the mixture was not measured accurately because it was just a separation trial. The mixture of the two compounds was homogeneous so they are miscible. Before the analysis the column was conditioned at 300 °C for 30 minutes.

Though the two compounds are very similar and have close boiling points, the separation was possible and the chromatogram is reported in Figure 3.15. The compound corresponding to each peak was identified by comparing the retention time of the peak with the retention time of the peak obtained by injecting the pure compound.

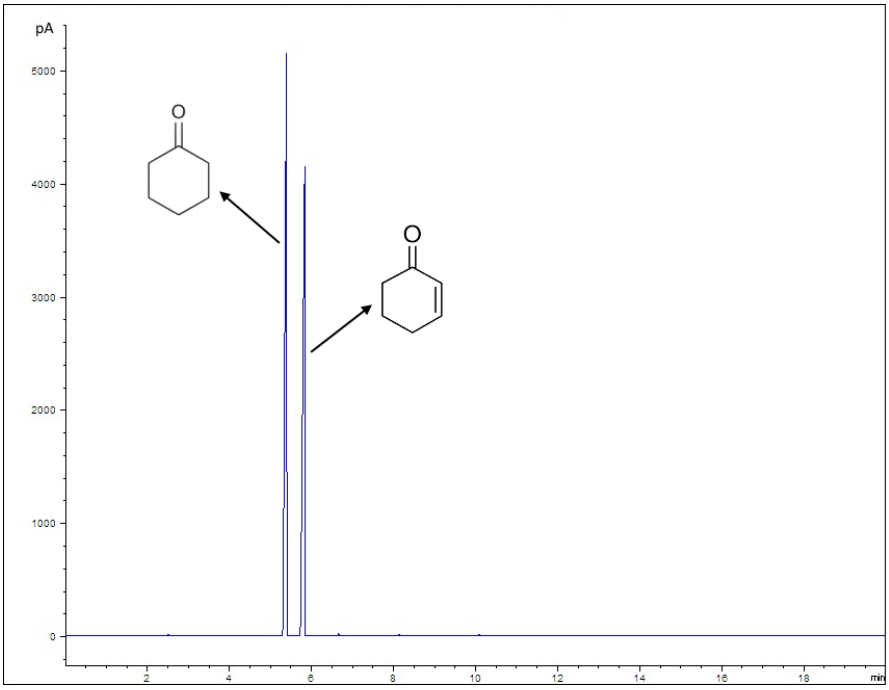

Figure 3.15. *Chromatogram of a 1:1 volume mixture of GI and API, with the GC-set-up 1.*

After the successful separation, some standard solutions of 2-cyclohexen-1-one (GI) in cyclohexanone (API) were prepared in order to plot a calibration curve for the concentration of the 2-cyclohexen-1-one. The concentration of the standard solutions, expressed in ppm weight of 2-cyclohexen-1-one in cyclohexanone are: 0 (blank), 2, 10, 25, 50, 75, 100, 125, 150, 200. The overlapped chromatograms of the standard solutions and the calibration curve are shown in Figure 3.16 and 3.17 respectively.

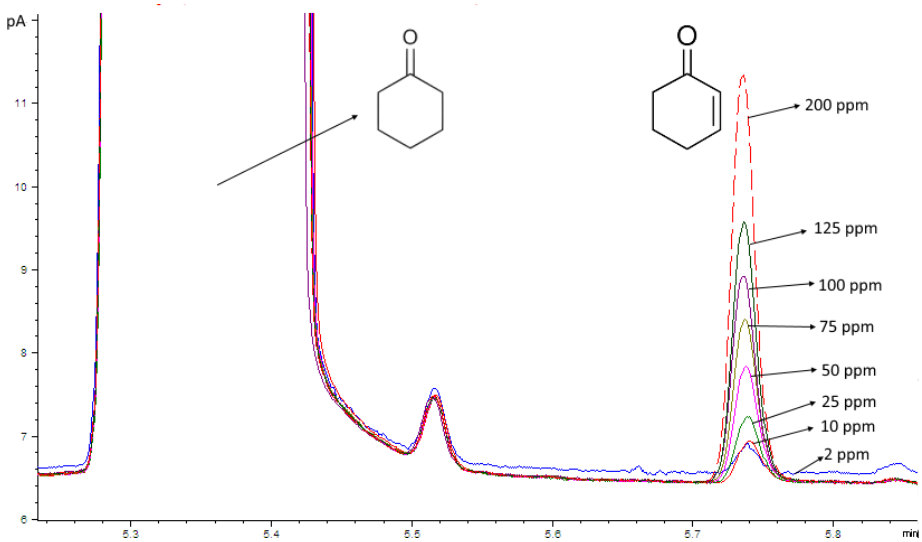

Figure 3.16. *Overlapping chromatograms of the standard solutions of GI in API for the first calibration curve. The GC-set-up 1 was used.*

Two observations can be done, about Figure 3.17:

- there is a linear relationship between the concentration of the GI and the peak area;
- the straight line obtained doesn't intercept the origin of the axes.

This means that in the blank standard (pure cyclohexanone) there are some ppm levels of 2-cyclohexen-1-one.

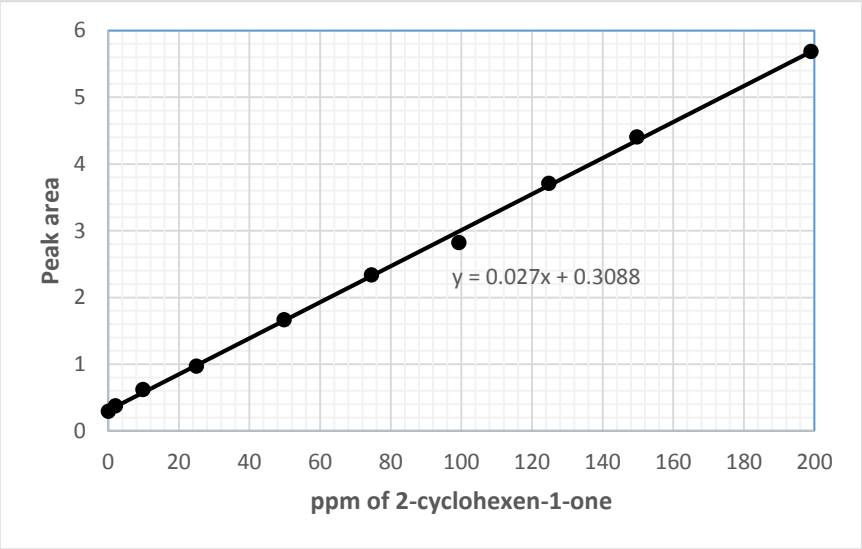

Figure 3.17. *First 2-cyclohexen-1-one calibration curve. The GC-set-up 1 was used.*

For this reason the calibration curve has been repeated using n-octane instead of cyclohexanone as solvent. The reasons to select the n-octane is its low volatility ($nbp_{n-octane} = 125\ ^{\circ}C$, the errors in the standard solutions preparation due to the evaporation of the compounds are minimized), it did not have impurities with the same retention time of the 2-cyclohexen-1-one and it does not react with the GI. In this case, for computing the calibration curve, the concentration of the GI was expressed in molarity (mol/L) instead of ppm weight. Using this unit of measure the curve is valid for determining the concentration of the 2-cyclohexen-1-one in every substance, if it is in the range covered by the standard solutions.

Before proceeding with the new calibration curve, we decided to modify the set-up of the GC to obtain 5 minutes shorter analysis time and a higher detection limit. The parameters values of the new set-up (set-up 2) are listed in Table 3.5.

The standard solutions that were prepared for the new calibration curve are listed in Table 3.6. The number of standard solution at low concentration was increased, the range was extended to higher concentrations and each standard solution was injected three times in the GC to verify the reproducibility of the analysis.

Table 3.6. *Standard solutions used for the second calibration curve.*

Standard solution	C_{GI} [ppm weight of GI in n-octane]	C_{GI} [mol/L]
Blank	0	0
1	2	1.52E-5
2	10	7.30E-5
3	17	1.24E-4
4	25	1.84E-4
5	37	2.70E-4
6	50	3.67E-4
7	75	5.46E-4
8	100	7.25E-4
9	119	8.68E-4
10	149	1.09E-3
11	199	1.46E-3
12	300	2.20E-3
13	400	2.91E-3
14	485	3.55E-3
15	598	4.37E-3
16	700	5.12E-3

The new calibration curve is shown in Figure 3.18.

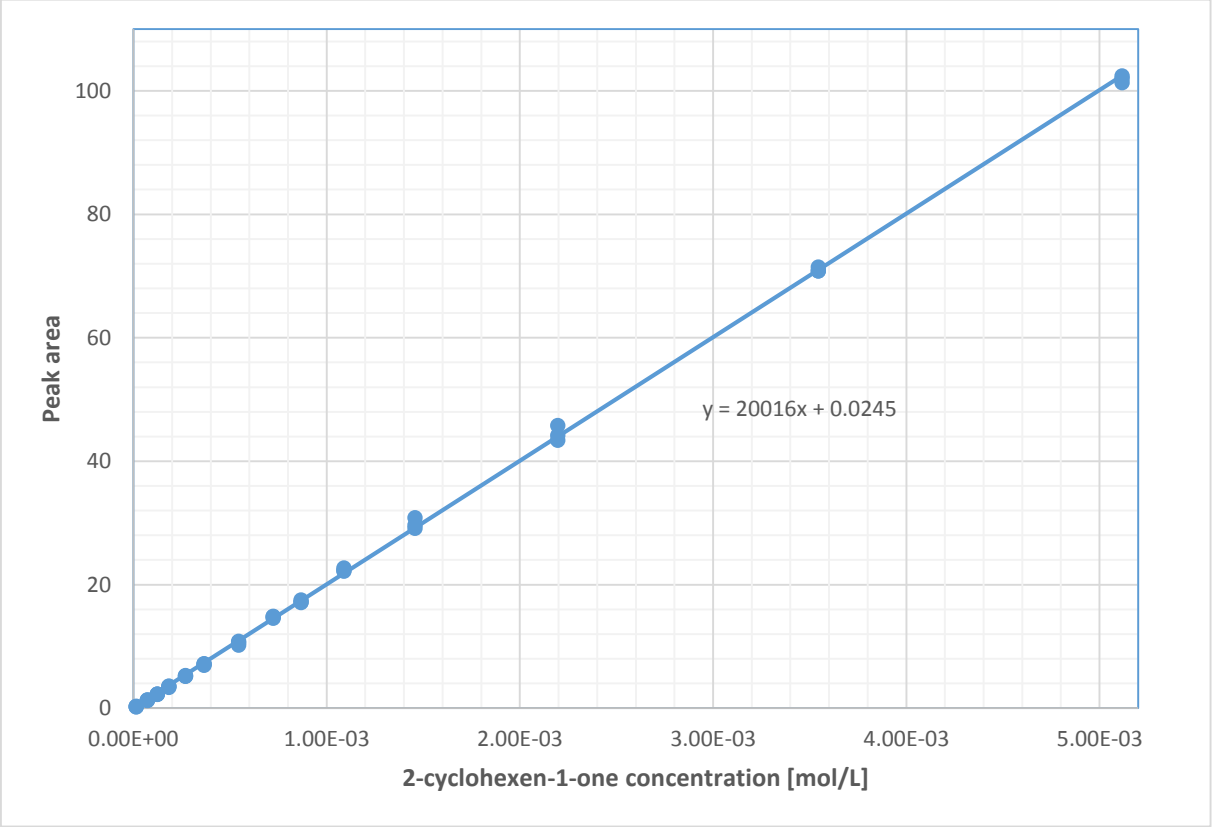

Figure 3.18. *Second 2-cyclohexen-1-one calibration curve.*

The new calibration curve obtained is still a straight line but now it passes through the origin of the axes. The reproducibility of the analysis is very good: for most of the standard solutions the three points corresponding to the three GC analysis are overlapped. For very few standard solutions the area measured is a bit different but this is probably due to some injection errors or other random errors.
This calibration curve was used in the successive experiments to determine the concentration of the 2-cyclohexen-1-one during the reaction.

3.2.4 Experimental design

After the set-up of the analytical method described in the previous paragraph, the desired reaction of Figure 3.5 have been tried first in small glass flasks agitated with the magnetic stir bar. Since the 2-cyclohexen-1-one represents an impurity, we started with an initial concentration around 500 ppm.
Once the reaction conditions have been optimized, the performances of the RBR were compared with those of the STR at different stirring rates. The scavenger used is always the one with the largest particle size of 200-500 μm except in the last experiment in which different particle sizes were used to investigate the internal mass-transfer.

3.3 Results and discussion

In this section the experiments are explained in detail and the results shown and discussed.

3.3.1 Optimization of the reaction conditions

All the reactions reported in this paragraph were carried out in small volume glass flasks, mixed with a magnetic stir bar at the highest rotation speed allowable to keep the stir bar stable. The scavenger used was the one with the largest diameter (200-500 μm).
All the experiments discussed to this paragraph and the relative reaction conditions are listed in Table 3.7.

Table 3.7. *List of the experiments from Exp.1 to Exp. 6*

Exp. #	Liquid vol. [mL]	T [° C]	Solvent	C_{GI}^0 [mM]	C_{GI}^0 [ppm w]	C_{API}^0[ppm]	GI:TG:B (molar ratio)	X_{GI} (t = 24 h)
1.1	7.4	21	Cyclohexanone (API)	3	300	-	1:6.1:0	0
1.2	7.4	80	Cyclohexanone (API)	3	300	-	1:6.1:0	0
2.1	11.2	21	tetrahydrofuran	6.9	750	630	1:6.1:0	0
2.2	10.6	21	dimethylformamide	4.9	500	630	1:12.2:0	0
2.3	10.6	80	dimethylformamide	4.9	500	630	1:12.2:0	0.14
2.4	12.7	21	acrylonitrile	5.3	640	640	1:9.4:0	0
2.5	7.5	21	dichloromethane	8.3	600	590	1:11.2:0	0
2.6	10.6	21	methanol	7.1	720	530	1:8.8:0	0.18
2.7	21	60	methanol	7.1	720	530	1:8.8:0	0.45
3.1	10.6	21	Cyclohexanone (API)	5.2	525	-	1:0:30.8	0
3.2	10.6	21	Cyclohexanone (API)	5.2	525	-	1:14.9:0	0
3.3	10.6	21	Cyclohexanone (API)	5.2	525	-	1:15.5:30.7	0.64
4.1	19.9	21	Methanol	4	490	520	1:0:8.2	0.4
4.2	19.9	21	Methanol	4	490	520	1:4:8.2	0.94
4.3	20.0	60	Methanol	4	490	520	1:0:8.2	0.36
4.4	19.9	60	Methanol	4	490	520	1:4:8.2	0.84
5.1	20.3	21	Ethanol	4.4	530	490	1:0:10.2	0
5.2	20.3	21	Ethanol	4.4	530	490	1:5.1:10.2	0.89
6.1	25.3	21	ethanol	4	490	0	1:9.2:17.6	0.98
6.2	22.8	21	30% w EtOH in API	5.1	560	-	1:0:16.1	0
6.3	22.8	21	30% w EtOH in API	5.1	560	-	1:8:15.7	0.77

The reaction have been tried first (Exp. 1) in neat conditions (without a solvent). The scavenger was added to a solution of 300 ppm of GI in API. From the scavenger capacity [mmol of thiol groups/g] is possible to calculate the scavenger mass corresponding to the desired number of moles of thiol groups (TG) needed.

As reported by Chen and Zhang (2005), in solid-supported solution-phase reactions like this, the advantage of easy separation can be counterbalanced by slow reaction, limitation on solvent selection, and the need to use large excess of the solid-bound reagent because not all the active sites on the solid-support are equally accessible.

For that reason we used an excess of scavenger (excess of thiol groups). The moles of TG added are reported as the proportion with respect to the moles of GI. The reaction was carried out at T = 21° C and T = 80° C. In both cases the GI conversion after 24 hours was 0.

Then we carried out the reaction with different solvents (Exp. 2) at T = 21° C and reduced the amount of the API to the same concentration of the GI in order to see if the API actually reacts with the scavenger.
The solvents considered were: dimethylformamide, tetrahydrofuran, dichloromethane and methanol, i.e. the most common for this type of applications.
The GI conversion after 24 hours was 18% with methanol and 0 with the other solvents
Two of the previous solvents, dimethylformamide and methanol, were tested at T = 21° C and also at higher temperature: T = 80° C and T = 60° C respectively. With dimethylformamide the conversion after 24 hours was 0 at T = 21° C and 14% at T = 80° C. With methanol 14% at 21° C and 45% at T = 60° C.
In all the experiments cited above, the cyclohexanone did not react.
From these experiments it is clear that in neat conditions there is no removal of the GI. Among the solvents tested only methanol gives interesting results, but the conversion could also be due to secondary reactions since the 2-cyclohexen-1-one is present in very low amount and could react with other impurities present in solution. Furthermore, even if the reaction was the desired one, it would be very slow.
The next step was to add a basic catalyst to facilitate the deprotonation of the thiol groups of the scavenger, as discussed in §3.1.3. The base used was the N,N-diisopropylethylamine (DIEA), that will be indicated with the letter B. Since it is a weak base, is necessary to use an excess of it with respect to the moles of TG in the reaction mixture.
The Exp.1 in neat conditions was repeated three times (Exp. 3) at T = 21° C:

- one time with only the TS;
- one time with only the DIEA;
- one time with the TS and the DIEA.

Only when TS and DIEA were both present the conversion of the GI was greater than 0 and equal to 64% after 24 hours. The corresponding time-conversion curve is shown in Figure 3.19.

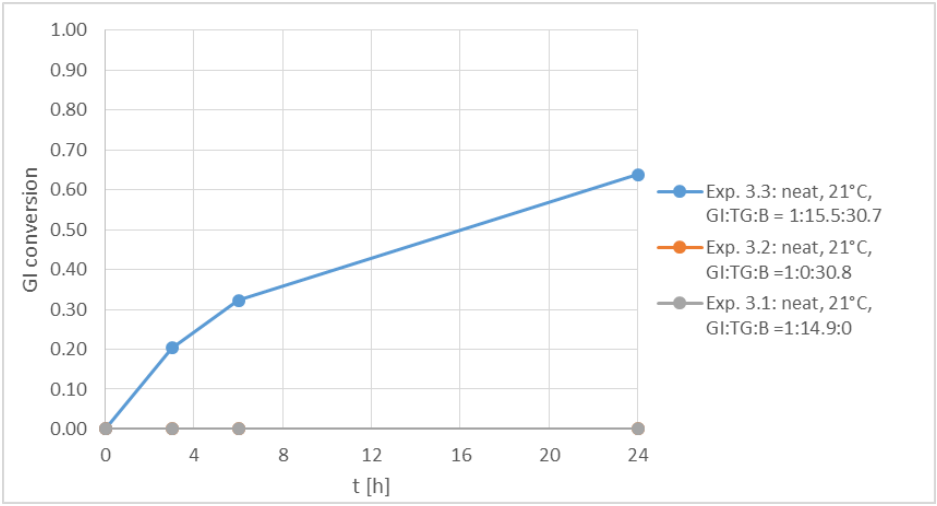

Figure 3.19. *GI conversion trend of Exp. 3.*

These experiments demonstrated that the addition of a basic catalyst is fundamental for promoting the reaction. Furthermore, there is no evidence of secondary reactions because when the TS is not present nothing reacts.
It seems that the curve of Figure 3.19 has not reached a flat plateau after 24 hours, suggesting that the conversion could have been higher if the reaction had been carried out for a longer time. Anyway it is important to underline that the 64% conversion after 24 hours was reached with a high excess of TG (15 times the moles of GI).

Afterwards, the reaction was carried out using methanol as solvent, plus the addition of the DIEA (Exp. 4). Two reactions were run in parallel, one with only DIEA and one with TS and DIEA, to detect any secondary reactions. Two temperature levels were investigated, T = 21° C and T = 60° C. The API was added in traces to verify that it did not react. The GI conversion curves are reported in Figure 3.20.
The fact that without TS the GI is converted rapidly to a value of 40% roughly indicates that the 2-cyclohexen-1-one undergoes one or more secondary reactions. For this reason the methanol is not a suitable solvent. When the TS is present the conversion arrives to 70% after 3 hours. At 24 hours the conversion is 94% at T = 21° C and 84% at T = 60° C, evidencing that the temperature has a negative effect on the reaction.
A second alcoholic solvent, ethanol, was subsequently tested. The experiment (Exp. 5) is analogue to the previous one, but at room temperature. The conversion is shown in Figure 3.20. With ethanol there are no side reactions in the absence of the TS and the conversion after 24 hours is quite high: 89%.

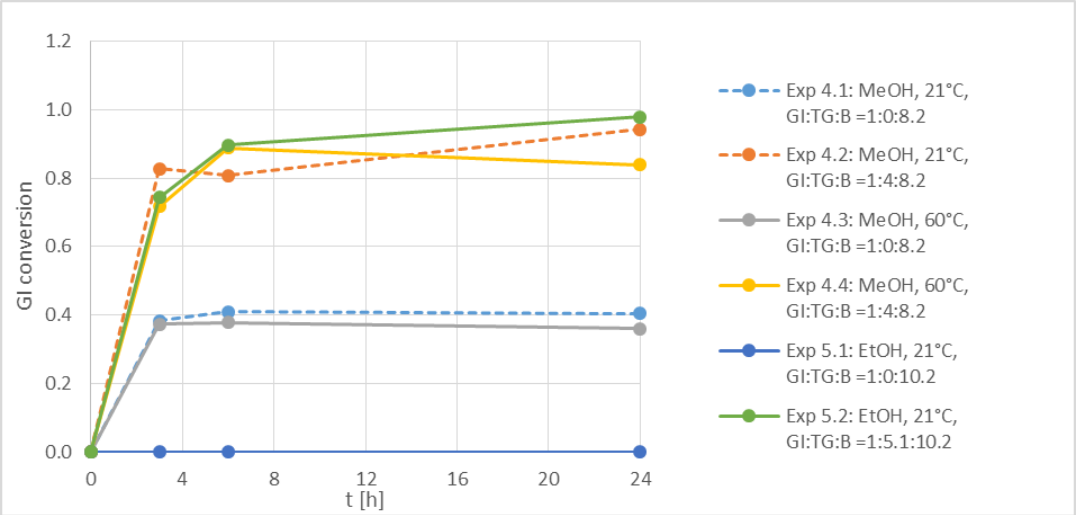

Figure 3.20. *GI conversion trend of Exp. 4 and 5.*

The absence of side reactions with ethanol is probably a consequence of its lower acidity with respect to methanol ($pK_{a,MeOH} = 15.5$, $pK_{a,EtOH} = 15.9$). The alcoxide ion formed after the deprotonation of an alcohol is in fact a nucleophile and it could react with the 2-cyclohexen-1-one in the same way of the thiol scavenger.

Finally, we tried to reduce the amount of ethanol and increase the API, using a mixture of 30% weight of ethanol in API as solvent (Exp. 6). The reaction was carried out with DIEA only and with DIEA and TS. The results, depicted in Figure 3.21, were compared with the ones obtained from the same reaction using only ethanol as solvent. Figure 3.21 suggest that the lower concentration of ethanol with respect to the API, the reaction slows down and the conversion after 24 hours is 77% instead of 98% when pure ethanol is used.

The explanation to this phenomenon could be that the ethanol, like methanol, is a protic solvent that promotes rapid proton transfer (see reaction mechanism of Figure 3.8) and stabilizes charged intermediates, this translates in a faster reaction. Thus, when the concentration of the protic solvent is reduced, also its effects are reduced.

In all the experiments made the API did not react.

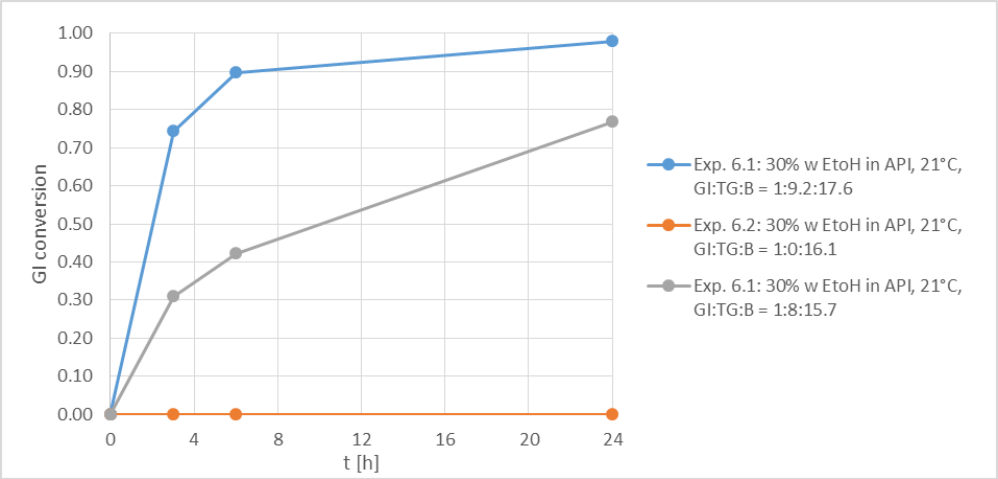

Figure 3.21. *GI conversion trend of Exp. 6.*

After these experiments, we decided to use pure ethanol as solvent in combination with the catalyst DIEA for the following reactions.

By keeping the same reaction conditions and varying only the parameters of interest, the effect on the reaction rate of the DIEA concentration (Exp. 7), TS amount (Exp. 8) and temperature (Exp. 9) was investigated. The details on these experiments are reported in Table 3.8 and the graphical results in figure 3.22 a), b) and c) respectively.

Table 3.8. *List of the experiments from Exp. 7 to Exp. 9*

Exp. #	Liquid vol. [mL]	T [° C]	Solvent	C_{GI}^0 [mM]	C_{GI}^0 [ppm w]	GI:TG:B (molar ratio)
7.1	19	21	ethanol	2.5	300	1:7:35
7.2	19	21	ethanol	2.5	300	1:7:72
7.3	19	21	ethanol	2.5	300	1:7:107
8.1	19	21	Ethanol	2.5	300	1:3.5:70
8.2	19	21	Ethanol	2.5	300	1:7:70
8.3	19	21	Ethanol	2.5	300	1:11:70
9.1	19	21	Ethanol	2.5	300	1:7:70
9.2	19	47	Ethanol	2.5	300	1:7:70
9.3	19	75	ethanol	2.5	300	1:7:70

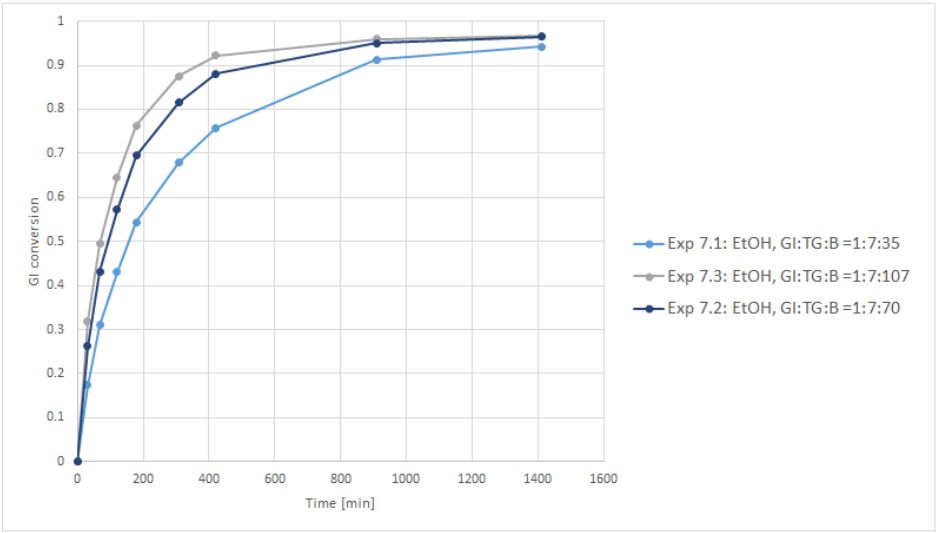

a)

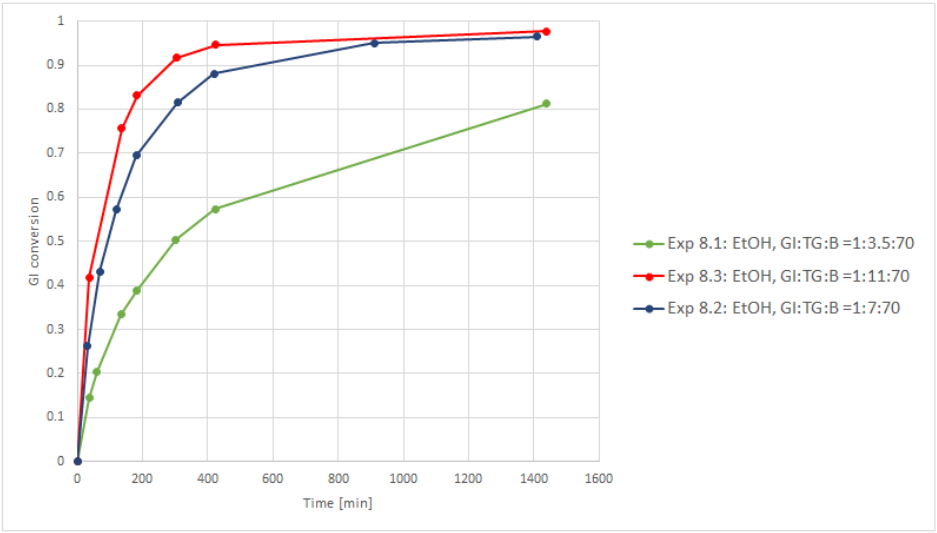

b)

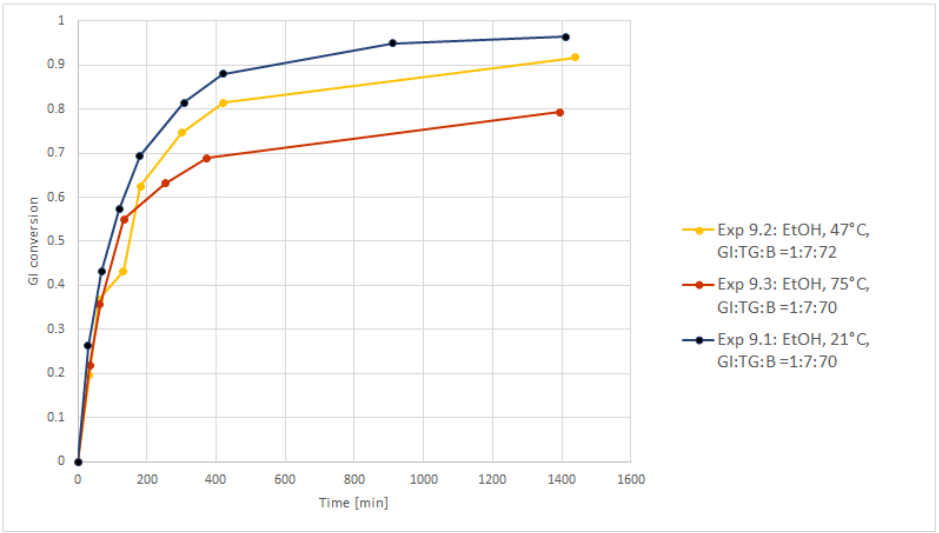

c)

Figure 3.22. *a) GI conversion trend of Exp. 7. b) GI conversion trend of Exp. 8. c) GI conversion trend of Exp. 9.*

From Figure 3.22 a) it is clearly noticeable that the reaction rate increases with the DIEA concentration also when large excesses of DIEA are used. The TS amount has also a positive effect on the reaction rate.
Conversely, it appears from Exp. 5, that the final conversion (after 24 hours) of the GI decreases with the temperature. One explanation could be the presence of a reaction equilibrium which is shifted towards the reactants as the temperature increases.
The optimal reaction conditions for the reaction are then the use of ethanol as solvent, a large excess of TS, DIEA as catalyst (in large excess with respect to the TG) and room temperature.

3.3.2 Rotating bed reactor vs. stirred tank reactor

From the previous experiments made in the small glass flasks, the optimal reaction conditions (solvent, initial concentration of GI, amount of TS, amount of DIEA, temperature) have been selected. The reaction was then carried out in the SpinChem® RBR S221 at different stirring rates: 200 rpm, 400 rpm and 800 rpm. The same was done using a normal STR, keeping the same vessel and replacing the rotating bed cell with a 4 pitched-blade impeller. In this case the scavenger was added directly in the liquid mixture, yielding a slurry. With the STR, the complete suspension of the solid was difficult at 200 rpm; the minimum stirring speed selected was 250 rpm instead of 200 rpm. For the same reason, the height of the impeller from the bottom of the vessel was lowered to 5 mm instead of 12 mm.
The same reaction has been tested also in a small glass flask agitated with the stir bar, both at low rotation speed of 100 rpm and at the maximum rotation speed possible at which the stir bar was still stable.
The characteristics of the reactors used are reported in §3.2.2.
The reaction conditions are reported in Table 3.9 and the conversion-time curves in Figure 3.23.

Table 3.9. *Experimental conditions used in the RBR – STR comparison.*

Reactor	Rotation speed [rpm]	Liquid vol. [mL]	T [° C]	Solvent	C_{GI}^{0} [mM]	C_{GI}^{0} [ppm w]	GI:TG:B (molar ratio)	Height of the rotating bed/impeller base from the vessel bottom [mm]
RBR	200, 400, 800	190	21	ethanol	2.5	300	1:7:105	12
STR	400, 800	190	21	ethanol	2.5	300	1:7:105	12
STR	250	190	21	ethanol	2.5	300	1:7:105	5

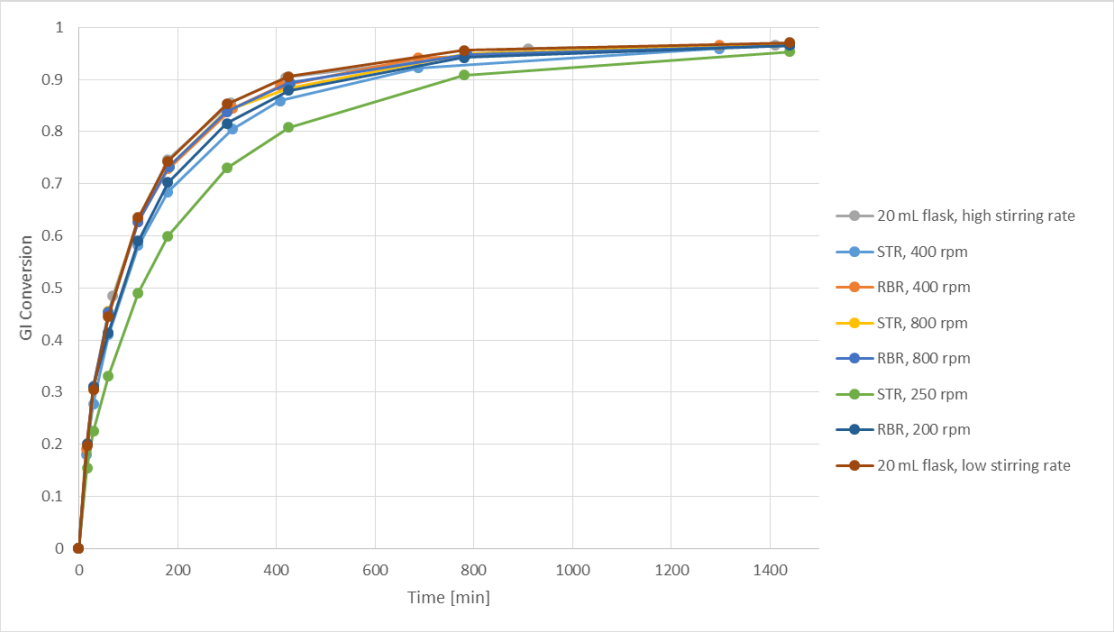

Figure 3.23. *Conversion curves obtained with the RBR and the STR at different rotation speeds.*

All the curves of Figure 3.23 are overlapped. The only exception is the STR at 250 rpm, whose reaction is a bit slower than the others. However this is likely due to the fact that some scavenger was trapped in the small cavity formed by the drainage hole at the bottom of the tank, hence it was not in good contact with the solution.

We conclude that neither the rotation speed nor the reactor type affect the reaction rate. Since these variables affect only the mass transfer in the external film surrounding the solid particles, the reaction appears not externally mass-transfer limited.

From this and the also the previous experiments is also important to note that the GI final concentration after 24 hours, expressed in ppm of GI in ethanol, is around 10 ppm, as the desired value. Anyway, as demonstrated with Exp. 3, if cyclohexanone is used instead of ethanol, the reaction is much slower and the desired final concentration of GI is not reached after 24 hours.

3.3.3 Internal mass transfer investigation

Since the TS is porous and has been verified that the reaction is not externally mass transfer limited, the presence of an internal-mass transfer limitation was investigated by running the reaction using scavengers of different particle size. All three particle sizes available listed in Table 3.3 were tested. All the other reaction conditions were kept constant and are reported in Table 3.10. Since the scavengers with different particle size do not have the same capacity (mmol of TG/g), the mass of scavenger added was recalculated, based on the scavenger capacity in order to add always the same moles of TG.

Table 3.10. *Experimental conditions used for the different particle size comparison.*

Particle diameter (d_p) [µm]	Liquid vol. [mL]	T [° C]	Solvent	C_{GI}^0 [mM]	C_{GI}^0 [ppm w]	GI:TG:B (molar ratio)
40-63	20	21	ethanol	2.5	300	1:14:210
120-200	20	21	ethanol	2.5	300	1:14:210
200-500	20	21	ethanol	2.5	300	1:14:210

The reactor used is the small agitated flask because it was demonstrated in the previous experiment that it is equivalent to the other types of reactor. A large excess of scavenger and DIEA were added in order to simplify the calculations for further modelling of the reaction kinetics. The results are shown in Figure 3.24.

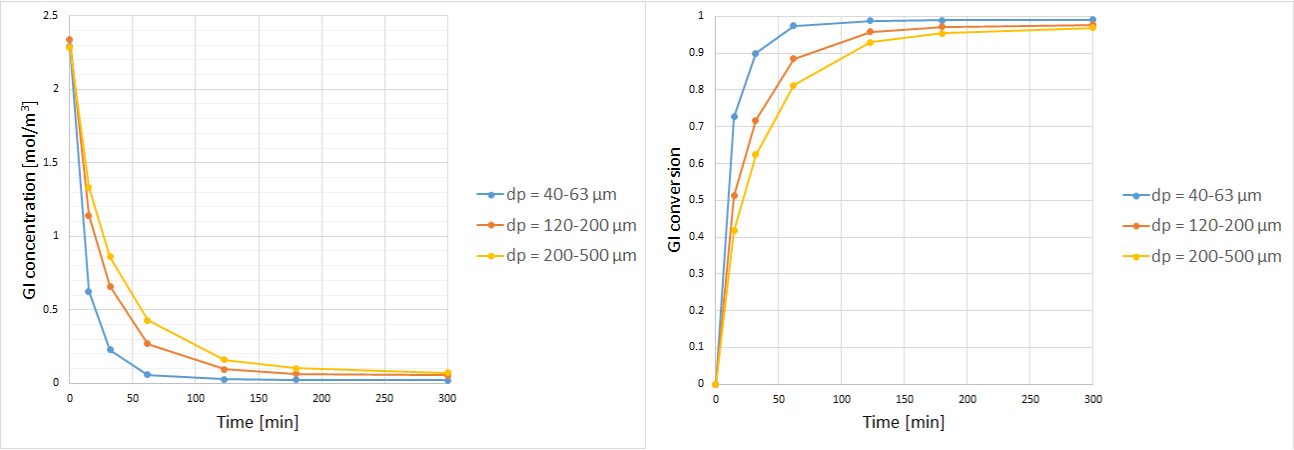

Figure 3.24. *GI concentration and conversion curves versus reaction time obtained with particles of different size.*

From Figure 3.24 is clear that the reaction rate is inversely proportional to the particle size. As said in §1.2.2 this suggests that the reaction is internally mass-transfer limited. That is also intuitive given that TS is porous and the rate of reaction is fast compared to the diffusion time in a porous matrix.

A more quantitative understanding has been developed through a modelling of these experiments.

The GI is now indicated with the letter A to simplify the notation. Since from the previous experiments of § 3.3.2 is clear that the reaction is not externally mass transfer limited, is possible to remove the terms regarding the external mass transfer from the material balance equations and the concentration of the GI at the external surface of the solid particles, C_A^i, can be considered equal to the GI concentration in the bulk, C_A^b.

For these reasons the material balance assuming perfectly stirred, closed reactor model, reduces to equation (1.4):

$$\dot{n}_A^{cons} = \frac{\mathrm{d}C_A^b}{\mathrm{dt}} = r_A'' \eta a^{L,tot} \quad . \tag{3.1}$$

The models tested for R'' and the respective expressions of ϕ and η used are the following:

$$1)\ R'' = k'' C_A^b \quad , \ \eta = 1 \quad , \tag{3.2}$$

$$2)\ R'' = k'' C_A^b, \ \phi = L\sqrt{\frac{k'' a^{S,tot}}{\mathfrak{D}_e}} \quad , \quad \eta = \frac{1}{\phi}\left(\frac{1}{tanh(3\phi)} - \frac{1}{3\phi}\right) \quad , \tag{3.3}$$

$$3)\ R'' = k'' {C_A^b}^n \quad , \quad \eta = 1 \quad , \tag{3.4}$$

$$4)\ R'' = k'' {C_A^b}^n, \phi = L\sqrt{\frac{(n+1)k'' a^{S,tot} {C_A^b}^{n-1}}{2\mathfrak{D}_e}} \quad , \quad \eta = \frac{1}{\phi}\left(\frac{1}{tanh(3\phi)} - \frac{1}{3\phi}\right) \quad , \tag{3.5}$$

where $k'' a^{S,tot} = k'''$. The parameters to be estimated are $k''$and n.
The detailed explanation of the previous models can be found in Chapter 1.
The assumption is that the reaction rate can be expressed as a function of the concentration of only GI (=A) because:

- the concentration of the DIEA, the catalyst, is constant and can be incorporated in k'';
- the scavenger is present in large excess and the superficial concentration of the TG can be considered constant and incorporated in k''.

To calculate $a^{S,tot}$ (see § 1.1.2), the density of the solid particles including the volume of the pores, ρ_p, has been calculated before. It is given by the ratio between the total mass of scavenger, m_s, and the total volume of the solid particles including their porosity, $V^{p,tot}$. It can alternatively be expressed as a function of the fused silica density ($\rho_{fs} = 2200\ kg/m^3$) and the specific pore volume of the scavenger, (S_a and spv respectively):

$$\rho_p = \frac{m_S}{V^{p,tot}} = \frac{1}{\frac{1}{\rho_{sil}} + spv} \quad . \tag{3.6}$$

The value of $a^{S,tot}$ has been calculated from the solid particles density, ρ_p, and the specific surface area of the scavenger, S_a:

$$a^{S,tot} = \frac{A^{tot}}{V^{p,tot}} = \frac{S_a m_S}{V^{p,tot}} = S_a \rho_p \quad . \tag{3.6}$$

For the calculation of the effective diffusion coefficient, equation (1.14):

- $\mathfrak{D}_{A,L}$ has been estimated with the Wilke-Chang method (Poling, Prausnitz and O'Connell, 2001). $\mathfrak{D}_{A,L} = 9.66e-10\ m^2/s$;
- ε_p has been estimated by dividing the pore specific volume for the specific volume of the solid particles:

$$\varepsilon_p = spv * \rho_p \quad ; \tag{3.7}$$

$\varepsilon_p = 0.62$;

- for τ was chosen an average common value of 3.5 (Fogler, 2005).

For each model tested the parameters k'' and n have been estimated. They are reported in Table 3.10 along with the values of the objective function (FOB) obtained at the end of the optimization. The results of the fitting are depicted in Figure 3.25.

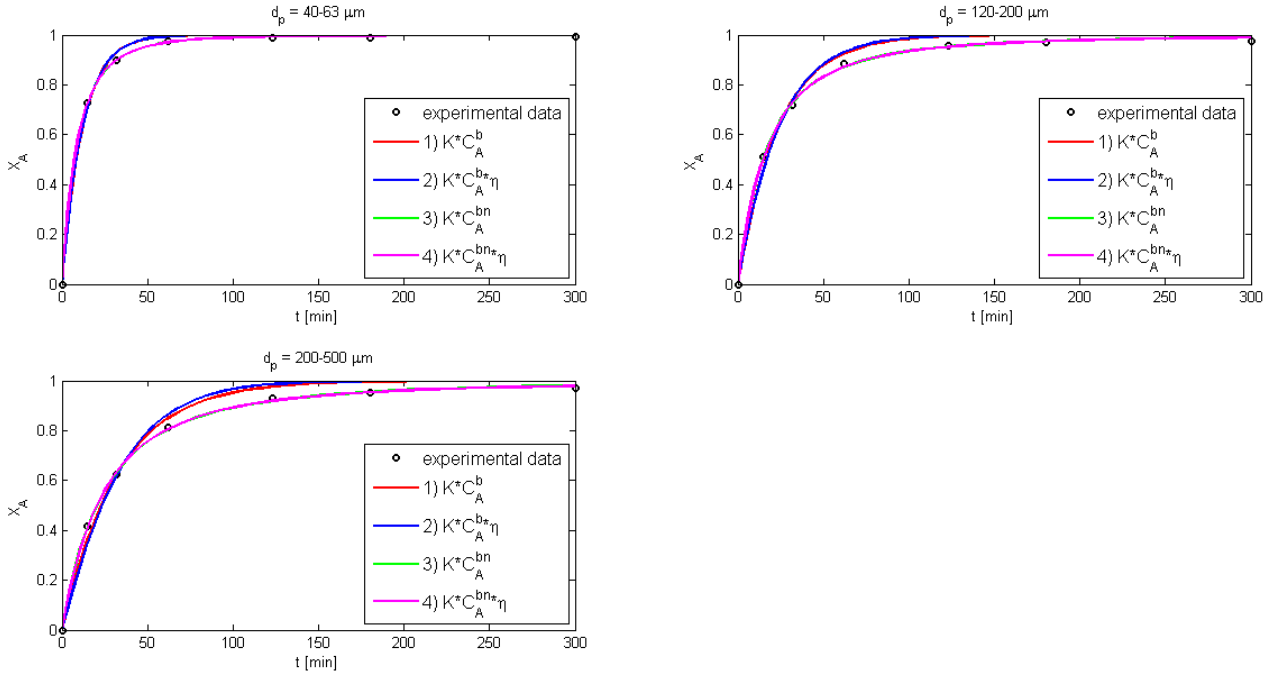

Figure 3.25. *Fitting of the experimental data obtained with the different particle sizes.*

Table 3.11. *Estimated parameters relative to the different particle sizes and the kinetic models used.*

d_p [µm]	Model	k''	n	FOB value
40-63	1	9.87e-11	-	0.04359
40-63	2	9.99e-11	-	0.04438
40-63	3	9.82e-11	1.35	0.01549
40-63	4	9.95e-11	1.35	0.01547
120-200	1	5.84e-11	-	0.08521
120-200	2	6.35e-11	-	0.09325
120-200	3	5.26e-11	1.48	0.02751
120-200	4	5.66e-11	1.51	0.02724
200-500	1	3.51e-11	-	0.09760
200-500	2	4.39e-11	-	0.11885
200-500	3	3.12e-11	1.50	0.02714
200-500	4	3.79e-11	1.58	0.02615

From the FOB values of Table 3.11 and Figure 3.25 is clear that the best models are models 3 and 4. The fitting and the estimated parameters of these two models are similar.

Using model 4 (that provides information about the internal mass transfer) and the estimated parameters, the values of the Thiele modulus and the effectiveness factor have been calculated as a function of C_A^b (since for *n*-th order reactions ϕ is a function of C_A^b), with C_A^b varying in the range of the experimental data. The effectiveness factor versus the Thiele modulus are plotted in Figure 3.26.

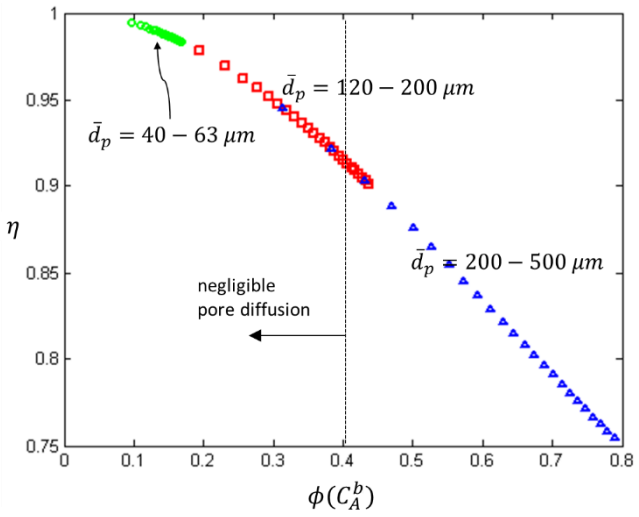

Figure 3.26. *Calculated effectiveness factors as a function of Thiele modulus obtained from the experiments using different particle sizes.*

Also the ratios of the observed rates of consumption of A obtained with the different particle sizes have been plotted against C_A^b in Figure 3.27. In the same figure the ratios of the average particle diameters are also reported.

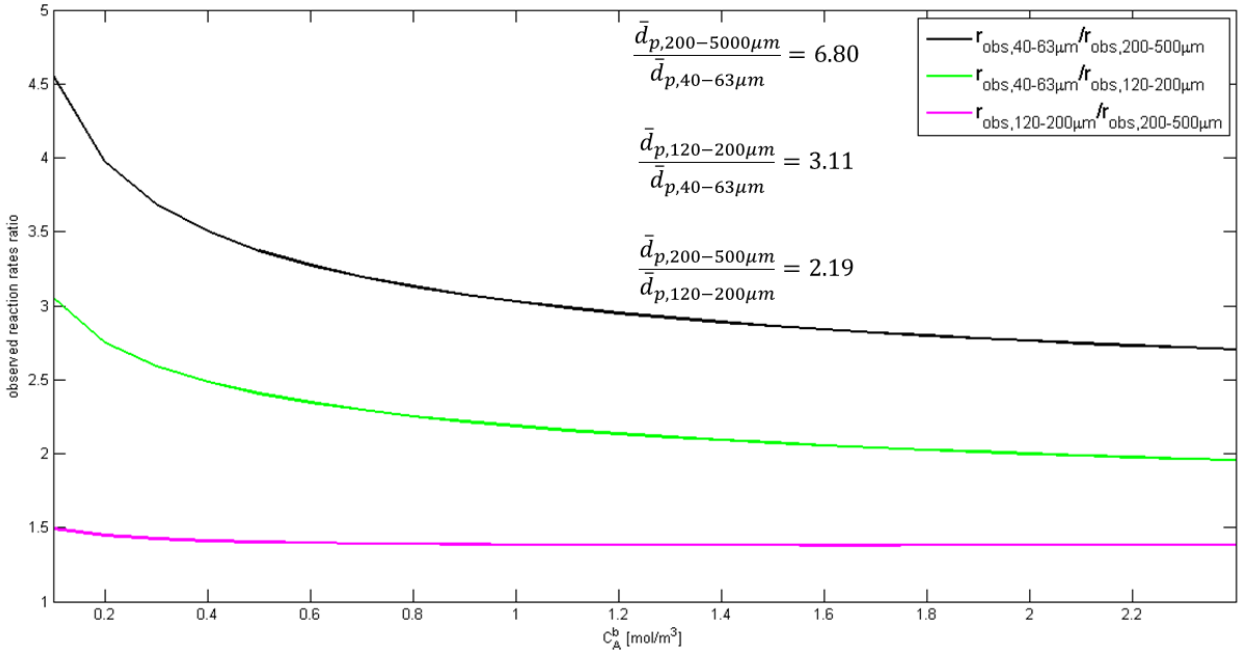

Figure 3.27. *Ratios of the observed consumption rates of GI relative to the different particle sizes.*

Figure 3.27 confirms that the Thiele modulus is inversely proportional to the particle size. With the smallest particles the estimated effectiveness factor is very close to 1 and $\phi < 0.2$, indicating that the pore resistance could be negligible in this case. With the intermediate particle size tested η is slightly lower and, for the highest values of C_A^b the Thiele modulus ϕ is greater than 0.4, the limit for negligible pores diffusion (Levenspiel, 1999). For the largest particle size, ϕ is always greater than 0.4 and its highest value is close to 0.8. Therefore in this last two cases the internal mass-transfer cannot be ignored and it seems in the same order of magnitude of the intrinsic chemical kinetics.

From Figure 3.27 is possible to see that the ratios of the observed reaction rates of the species A are not equal to the ratios of the average particle diameters, but somehow lower. This confirms that the reaction is not in the in the strong pores-diffusion regime ($\phi > 4$), though the effect of the porosity cannot be neglected.

However it has to be taken into account that the accuracy of these results is not very high, as a consequence of the inaccuracy of the kinetic model itself and the assumptions made. Among these, the most influential are:

- the solid particles have been assumed spherical, but their shape is irregular;

- the average diameter of the particles was used in the calculations, without taking into account any particle size distribution (it wasn't available);
- the estimation of ε_p is quite approximated;
- the value of τ have been chosen arbitrarily.
- The most reliable results are always the experimental ones and they say that the particle size has an effect on the reaction rate, likely due mostly to the internal diffusion inside the solid pores.

Chapter 4

Ion exchange reaction

This chapter is about the study of the RBR by using a solid-liquid ionic exchange reaction. A series of experiments oriented to the understanding of the reaction and the optimization of the reaction conditions and parameters was done first. Then the RBR and the normal STR were compared at different rotation speeds.
Finally, the importance of the type of baffles used and the height of the rotating bed (RB) in the vessel was investigated.

4.1 Theoretical aspects

The solid-liquid ion exchange reaction used is a very simple and common reaction. This kind of reaction is widely employed for the deionization of the water. The water flows through an ion-exchange resin bed and the ions of the dissolved salts are exchanged and replaced by H^+ and OH^- ions from the resin.
Ion exchange resins are polymers that are capable of exchanging particular ions within the polymer with ions in a solution that is passed through them. This ability is also seen in various natural systems such as soils and living cells.
The synthetic resins are used primarily for water softening, but also for various other applications including separating out some elements.
Ion exchangers are insoluble acids or bases which have salts that are also insoluble, and this enables them to exchange either positively charged ions (cation exchangers) or negatively charged ones (anion exchangers).
Most typical ion-exchange resins are based on crosslinked polystyrene. The actual ion exchanging sites are introduced after polymerisation. Additionally, in the case of polystyrene, crosslinking is introduced via copolymerisation of styrene and a few percent of divinylbenzene, like in Figure 4.1. Crosslinking decreases ion-exchange capacity of the resin and prolongs the time needed to accomplish the ion exchange processes but improves the robustness of the resin.

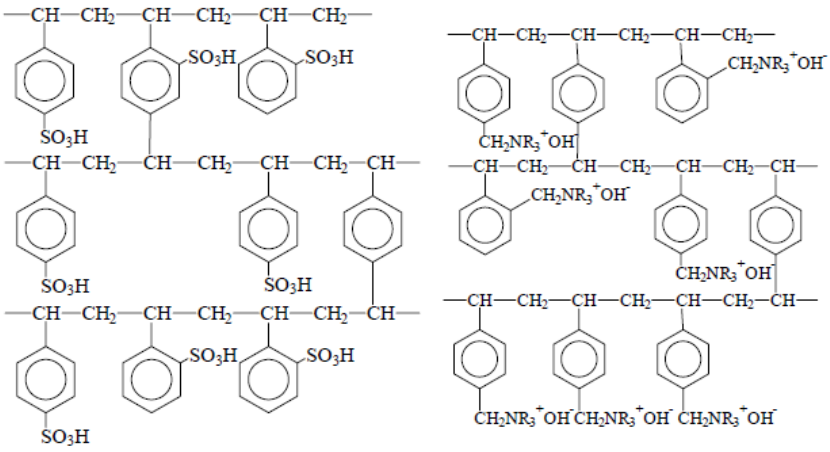

Figure 4.1. *Two common examples of ion-exchange resins.*

The resins are prepared as spherical beads of 0.5 to 1.0 mm in diameter. These appear solid even under the microscope (Figure 4.2 a)), but on a molecular scale the structure is quite open, (Figure 4.2 b)).

This means that a solution passed down a resin bed can flow through the crosslinked polymer, bringing it into intimate contact with the exchange sites.

Four main types of ion exchange resins differ in their functional groups:

- strongly acidic, typically featuring sulfonic acid groups, e.g. sodium polystyrene sulfonate;
- strongly basic, typically featuring quaternary amino groups, for example, trimethylammonium groups;
- weakly acidic, typically featuring carboxylic acid groups;
- weakly basic, typically featuring primary, secondary, and/or ternary amino groups, e.g. polyethylene amine.

The structure of the first two types of resin is shown in Figure 4.1.

Suppose a resin has greater affinity for ion B than for ion A. If the resin contains ion A and ion B is dissolved in the water passing through it, then the following exchange takes place, the reaction proceeding to the right (R represents the resin):

$$RA + B^{n\pm} \rightleftharpoons RB + A^{n\pm} \quad , \tag{4.1}$$

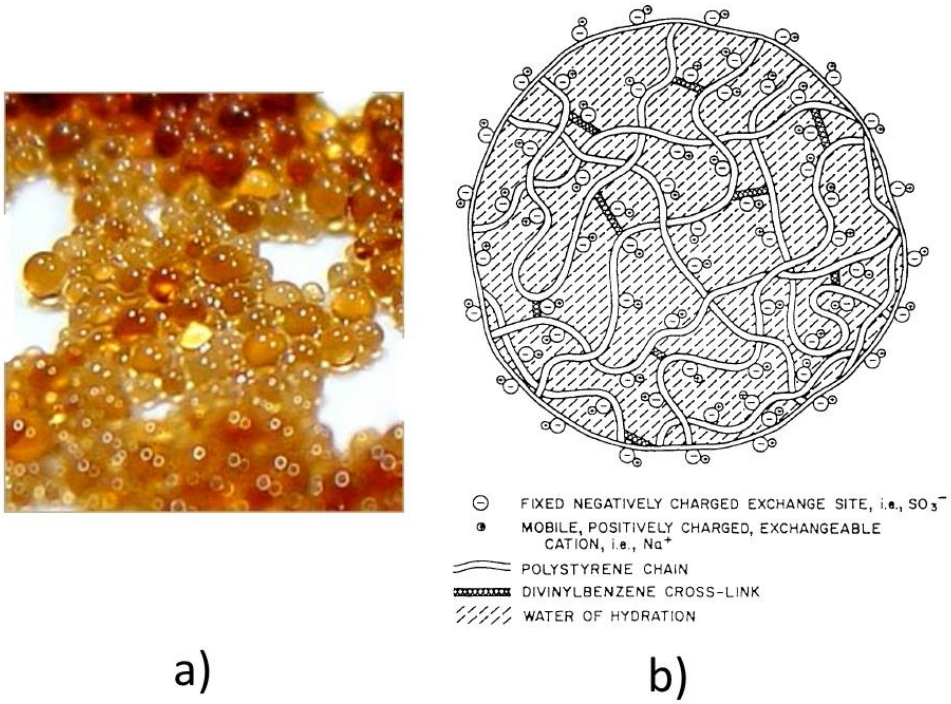

Figure 4.2. a) *Macroscopic and* **b)** *molecular structure of an ion-exchange resin.*

When the resin exchange capacity approaches exhaustion, it will mostly be in the RB form.

4.2 Instruments, materials and methods

This chapter describes the properties of the ion-exchange system used for this study (type of resin, ionic species to react with), the reactors and the analytical method used to measure the reaction time.

4.2.1 Substances

The ion-exchange reaction chosen is the one represented in Figure 4.3.

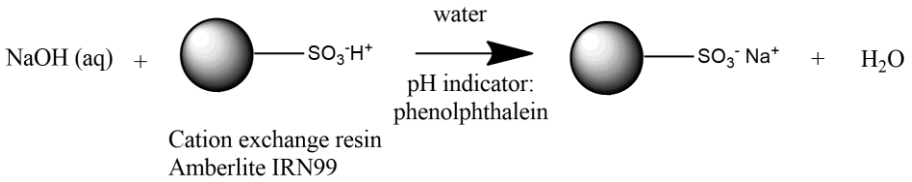

Figure 4.3. *Ion exchange reaction used to study the RBR.*

The cation exchange resin used is the Amberlite^{TM} IRN99 produced by DOW$^{®}$. Its properties are listed in Figure 4.4.

Physical form	Dark amber translucent beads
Matrix	Polystyrene divinylbenzene copolymer
Functional groups	Sulfonic acid
Total volume capacity (H+ form)	2.4 eq/L
Shipping density	840 g/L
Fines content < 0.300 mm, max	0.1%
Coarse content > 0.850 mm, max	1.0%
Uniformity coefficient, max.	1.2
Operating temperature	15-60°C

Figure 4.4. *Appearance and properties of the ion-exchange resin Amberlite IRN99.*

A 1.05 M NaOH solution was prepared by dissolving 4.2 g of NaOH in 100 mL of deionized water.

To follow the reaction phenolphthalein was used as pH-indicator. 40 mg of phenolphthalein were first dissolved in 0.5 mL of the previous 1.05 M NaOH solution and then added to 1 L of deionized water. Several liters of this solution were prepared.

Before use, a big amount of raw resin was washed six times with deionized water in a vacuum funnel. The volume of water used for each wash cycle was equal to the volume of resin to be washed. The vacuum was regulated so that the water flux through the resin was slow (the flux has not been measured, the washing time was around 5 min). During the wash the resin was always kept immersed in the water to ensure its wetting and prevent the air to enter in the pores of the beads. Also after the wash cycle, the clean resin was stored under deionized water in a glass bottle for the same reasons.

Washing of the raw resin is supposed to have two functions:

- wash away the impurities, such as salts or small amounts of acids, from the raw resin;
- force the air out from the beads pores, enhancing the wetting of the resin.

4.2.2 Reactors

The reactors used are the same described in §3.2.2 but more types of vessels, differing in diameter and type of baffles, were tested. They will be described later.

4.2.3 Experimental and analytical method

The characteristics of the phenolphthalein as pH indicator are reported in Figure 4.5.

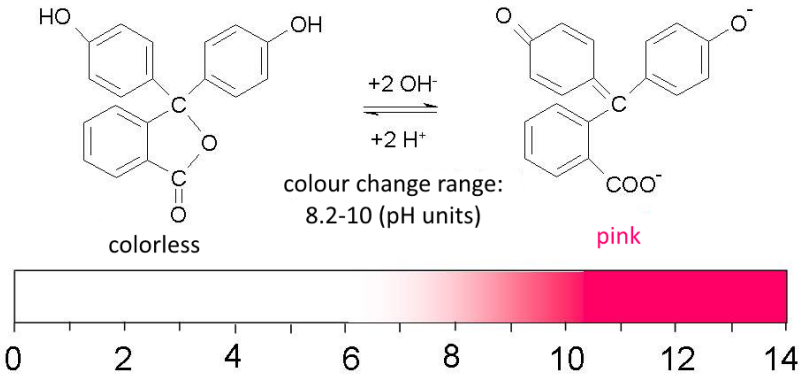

Figure 4.5. *Properties of the pH-indicator phenolphthalein.*

When the pH of the solution is lower than 8-8.2 the solution is clear. After the addition of a sufficient amount of a base, like NaOH, the colour suddenly shifts to the pink. If this basic solution flows through the cation exchange resin Amberlite IRN99 contained in the RB, the OH^- ions are removed from the solution and below pH = 10 the strong pink colour gradually fades. When the pH is lower than 8-8.2 the solution returns completely clear. The reaction can be repeated with the same batch of resin by adding again NaOH. OH^- builds up on the resin, up to saturation after many cycles.

The reaction time to achieve OH^- removal (from the initial pH to pH = 8-8.2) corresponds to the solution discoloration time after the NaOH addition and it can be measured visually, with a stopwatch or by using a probe connected to a spectrophotometer.

The procedure used for the experiments is the following one:

- the reactor is filled with the basic phenolphthalein solution (§ 4.2.1) and the ion-exchange resin is added;
- the stirring element (RB or impeller) is set in motion by switching on the overhead motor;
- when the solution is clear a small volume of the 1.05 M NaOH solution is added with the micropipette; this corresponds to the initial time;
- the reaction is allowed to run and just after the discoloration the final time is registered
- a new volume of NaOH can be added to run another reaction.

All the experiments were carried out at room temperature (21° C).

4.2.4 Experimental design

The experimental plan is divided in four series of experiments:

1. the reaction was carried out with *different volumes* of resin in the RB to see how the reaction time varies and decide the most convenient amount of resin to be used for the next experiments;

2. the *RBR and the STR* were compared at different rotation speeds;
3. the *position* (height) of the rotating bed in the vessel was varied to see if and how it influences the reaction time;
4. study of the effect of the *baffles type* (unbaffled vessels, vessels with normal baffles and flower-baffled vessels) and the *RB height* on the reaction time. Different *diameters* of the vessel were tested.

4.3 Results and discussion

The results of the four series of experiments summarized in the previous paragraph are here reported and discussed. The symbols and acronyms used are the following: V_L (liquid volume), V_R (resin volume), V_{NaOH} (injection volume of NaOH 1.05 m), RS (rotation speed), H_{RB} (height of the rotating bed base from the vessel bottom), H_I (= height of the impeller base from the vessel bottom), H_L (liquid height in the reactor), D_L (vessel diameter), D_{RB} (rotating bed diameter). The meaning of some of these abbreviations is also shown in Figure 4.6.

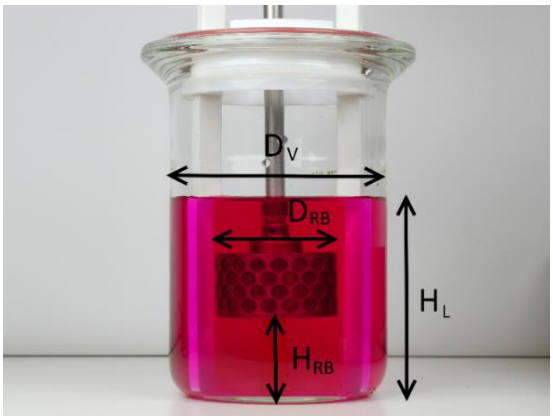

Figure 4.6. *Main geometrical parameters of the reactors used.*

4.3.1 Resin volume vs. reaction time

For these experiments the RBR shown in §3.2.2 was used. Different volumes of resin inside the reactor were tested. For each volume, several measurements of the reaction time were done by subsequent injections of the NaOH solution.

After each series of injections (experiment) with the same resin volume, both the phenolphthalein solution and the resin were substituted with fresh ones before the next experiment.

The details on the experiments are reported in Table 4.1 and the results in Figure 4.7.

Table 4.1. *List of the experiments and experimental conditions.*

V_L [mL]	V_R tested [mL]	V_{NaOH} [µL]	RS [rpm]	H_{RB} [mm]	Replications for each V_R
200	2.5, 5, 10, 20, 28	100	800	10	2

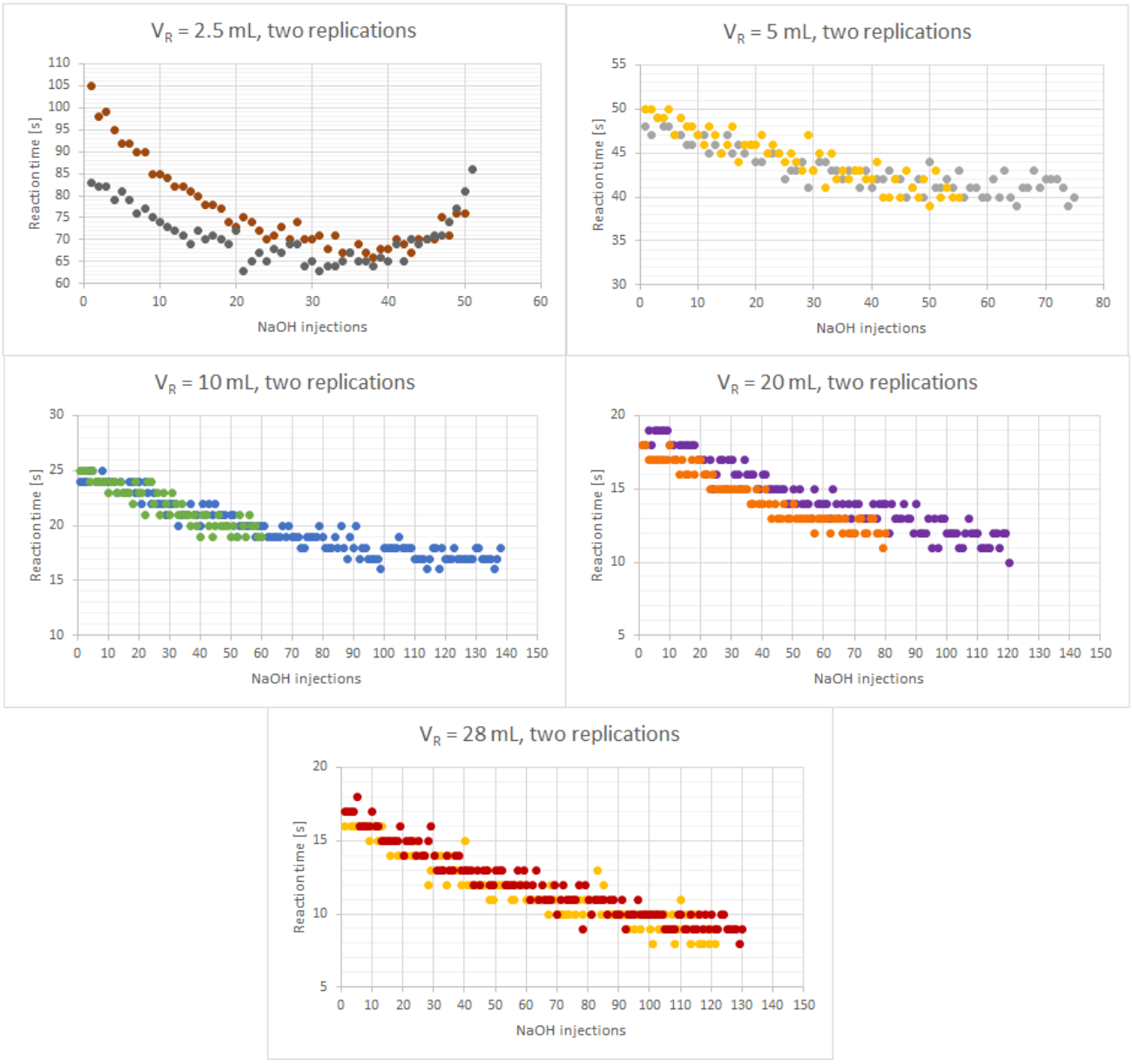

Figure 4.7. *Reaction time as function of the NaOH injections for different resin volumes.*

The results show that the experiments are repeatable. Measurements with the stopwatch become progressively less accurate as the reactions gets faster. Only with the smallest amount of resin tested (2.5 mL) the points corresponding to the two replicas are not exactly overlapped. Unexpectedly, the reaction time always decreases with the NaOH injections, above a minimum amount of resin. Possible causes are:

- the forced flow of liquid through the resin bed gradually increase the wetting of the resin beads and the solid-liquid contact increases;
- the swelling degree of the resin changes as a consequence of the substitution of the protons of the sulfonate groups of the resin with the Na^+ ions of the base due to the ion exchange.

The decrease in the reaction time is greater with 2.5 mL with respect to the other resin volumes. Always with this volume of resin, an increase of the reaction time is observed after 35-40 injections of NaOH. This is due to the saturation of the functional groups of the resin.

All the points of each graph of Figure 4.6 have been plotted as a function of the resin volume in Figure 4.8 a).

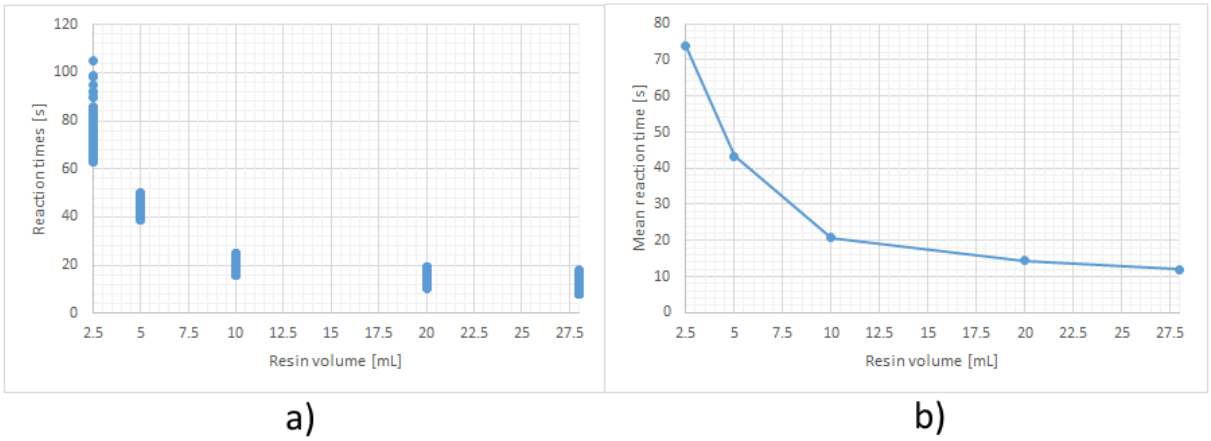

Figure 4.8. a) *Reaction times versus resin volume.*
b) *Mean reaction times versus resin volume.*

The time drift appears as a vertical dispersion. From the points of Figure 4.8 a), the mean reaction times corresponding to each volume of resin have been calculated and plotted as a function of the resin volume in Figure 4.8 b).

4.3.2 Rotating bed reactor vs. stirred tank reactor

From the previous series of experiments we decided to use a volume of resin of 5 mL for the next experiments. With this amount the reaction time is high enough (but not too high) and variations in other factors, like the rotation speed, will probably induce a detectable variation in the reaction time, if those factors have an impact on it. If a very high volume of resin was used the reaction time would be very low and changes in it due to the change of other variables would be probably too small to be measured by a stopwatch.
The RBR and the STR have been compared by running the ion exchange reaction at the same conditions in both the reactors. This was done for five different rotation speeds: 200 rpm, 400 rpm, 600 rpm, 800 rpm and 1000 rpm.

The experiments are summarized in Table 4.2 and the results reported in Figure 4.9, 4.10 and 4.11.

Table 4.2. *List of the experiments and experimental conditions.*

Reactor	V_L [mL]	V_R [mL]	V_{NaOH} [µL]	RS [rpm]	H_{RB} or H_I [mm]	Replications for each RS
RBR	200	5	100	200, 400, 600, 800, 1000	10	2
STR	200	5	100	200, 400	6	2
STR	200	5	100	600, 800, 1000	17	2

In Figure 4.9 the results, divided for rotation speed, are presented.
In Figure 4.10 the results of all the experiments are plotted together, but separated for reactor type. For both the RBR and the STR there is a clear dependence of the reaction time on the rotation speed, gradually vanishing at increasing rotation rate. This already suggests that the reaction is mass-transfer limited.
In Figure 4.11 a) the points obtained for each rotation speed are plotted against the corresponding rotation speed. For each speed tested, the reaction times of both replicas obtained with the RBR were compared with those obtained with the STR, using a non-parametric statistic test to assess if there was or not a significant difference between the two samples. As observable visually from Figure comparison it results that:

- the STR is better than the RBR at 200 rpm;
- the STR is the same as the RBR at 400 rpm;
- the RBR is better than the STR at 600, 800 and 1000 rpm.

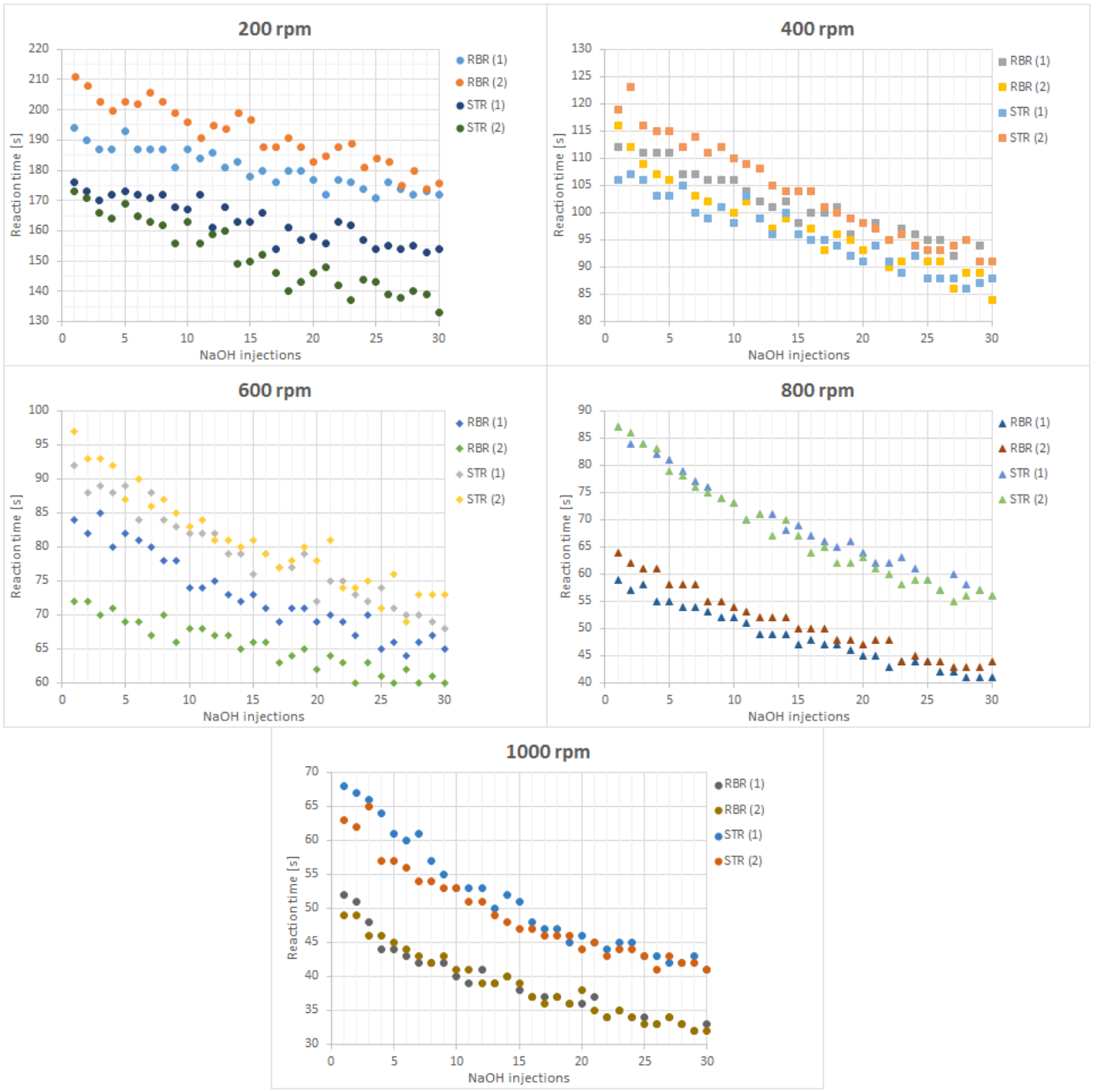

Figure 4.9. *Reaction times versus NaOH injections at each rotation speed tested.*

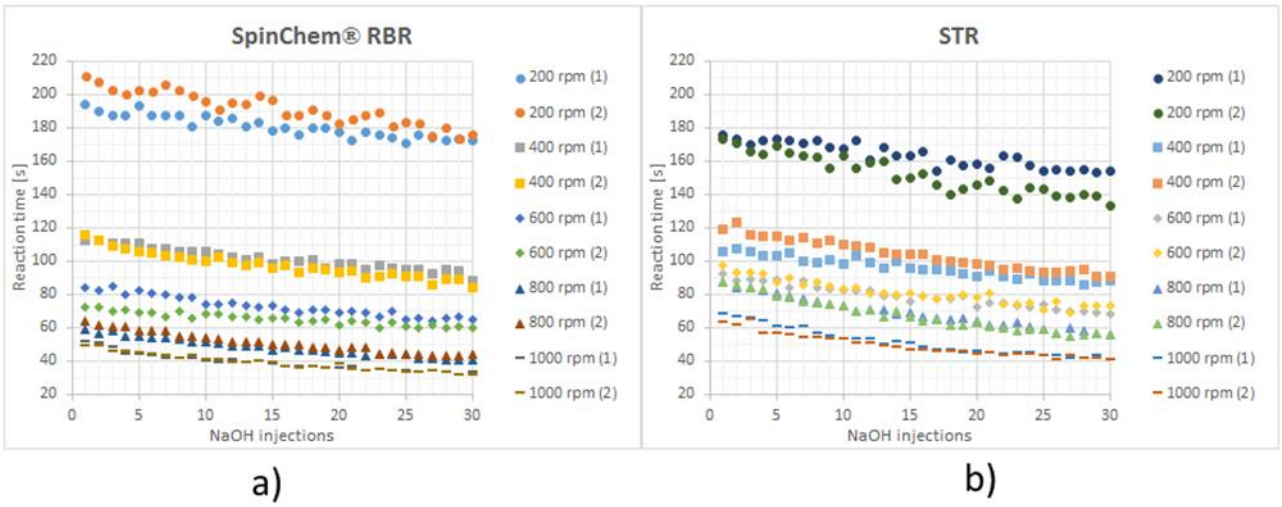

Figure 4.10. *Reaction times obtained* **a)** *with the RBR and* ***b)*** *with the STR at different rotation speeds as function of the NaOH injections.*

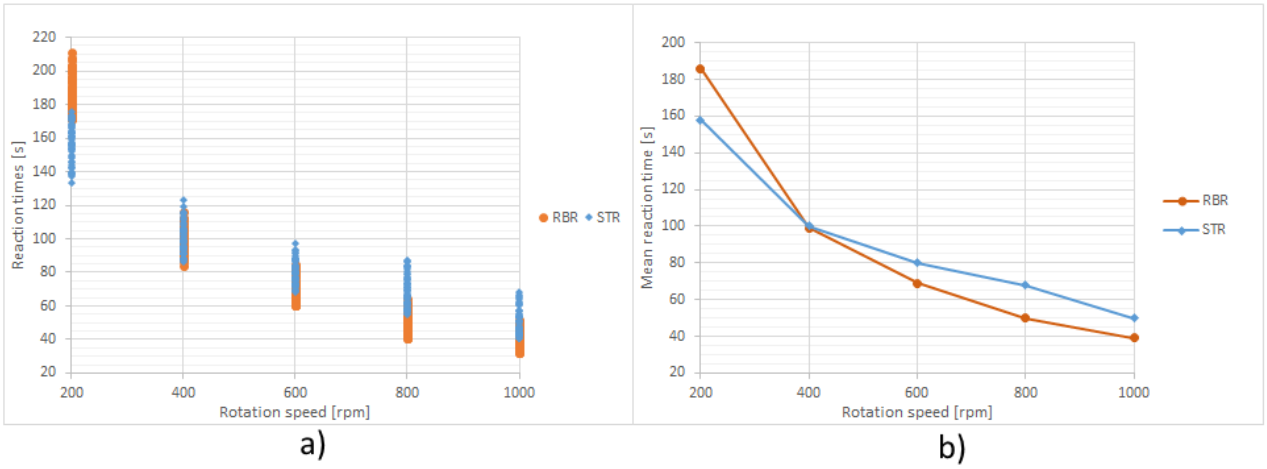

Figure 4.11. a) *Reaction times versus rotation speed.*
b) *Mean reaction times versus resin volume.*

4.3.3 Effect of rotating bed position

In these experiments the height H_{RB} (see Figure 4.6) of the RB from the bottom of the vessel was varied and the corresponding reaction time measured to see if there is a relationship between the two variables. The vessel used was the standard flower-baffled vessel described in § 3.2.2.

The position is the distance (or height) between the rotating bed base and the bottom of the vessel. As shown in Figure 2.3 a) and e) the RB has two small holes for the air outlet in the center of its upper part. When the RB rotates, a vortex is formed at the liquid surface. If the RB is too close to the liquid surface or H_L is too low, the center of the vortex can reach the two holes and the air is sucked-in, causing operating problems: during the spinning of the RB, the air can partially occlude the suction hole in the bottom of the RB, resulting in a lower liquid

flow through it. The maximum height, at fixed rotation speed, is thus defined as the height H_{RB} such that the eye of the vortex is very close to the two holes for the air outlet, like in the reactors of Figure 4.16. Inversely, the minimum height is when the RB base is almost touching the vessel bottom.

The procedure used is the following one:

- some NaOH injections (4 in this case) were made, and the reaction time measured, with the RB at the maximum height;
- the rotating bed height was decreased and other NaOH injections made at the new height;
- the previous step were repeated for the desired heights to test, every time decreasing the height.

The experiments are listed in Table 4.3 and the results reported in Figure 4.12 and 4.13.

Table 4.3. *List of the experiments and experimental conditions.*

V_L [mL]	V_R [mL]	V_{NaOH} [µL]	RS [rpm]	H_{RB} tested [mm]	NaOH inj. for each H_{RB}	Replications
210	5	100	500	24, 16, 8, 0	4	2

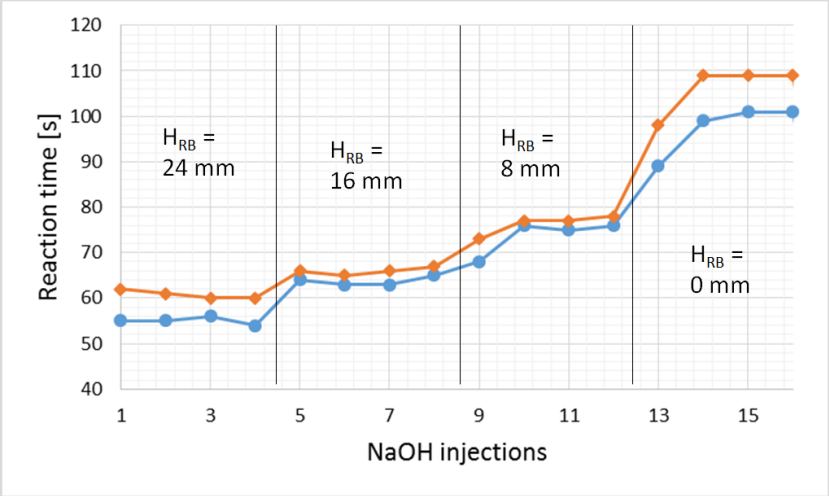

Figure 4.12. *Reaction time as function of the RB height and NaOH injections.*

The results show that the reaction time is inversely proportional to the bed height H_{RB}. This dependence is even a bit underestimated considering that the reaction time naturally tends to diminish when the number of NaOH injections increase, as shown from the previous series of experiments in § 4.3.2 and 4.3.1.

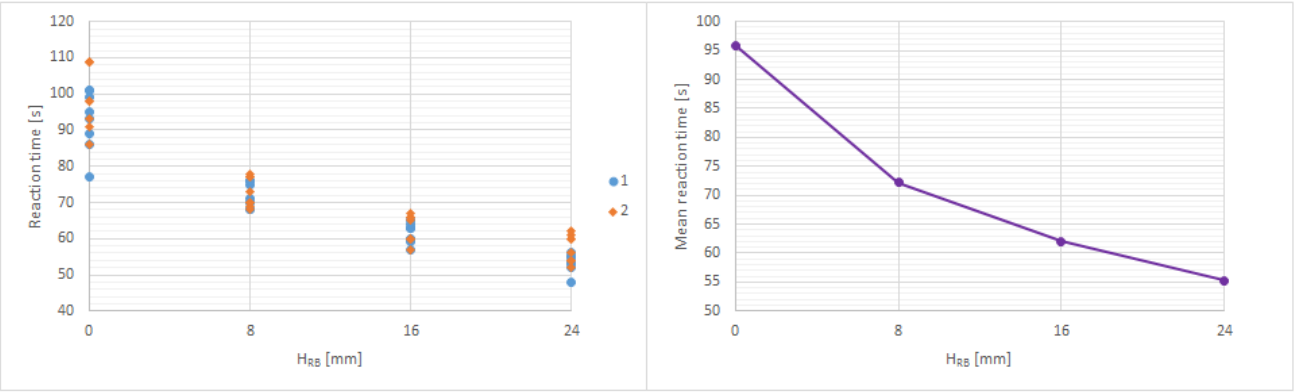

a) b)

Figure 4.13. a) *Reaction times versus RB height.* **b)** *Mean reaction times versus RB height.*

One explanation of this effect could be that the RB sucks the liquid almost only from the hole at its bottom and, for this reason, only the liquid below the RB is well mixed and easily enters in it. The liquid above the RB is more stagnant and cannot enter directly in it because on the top of the RB there are only the two small holes for the air outlet. Thus, the liquid that is above the RB has to migrate below the RB and then enter in it through the big hole. This effect is greater when the RB is very close to the bottom of the vessel because there is a lot of liquid above the RB (and much less below the mixer) that has to reach the lower part of the bed to enter in it. When the RB is very close to the bottom, the liquid must also overcome a greater pressure drops to enter in the RB because there is a very tiny clearance between the bottom of the vessel and the base of the RB.

4.3.4 Effect of the baffles type using the rotating bed

Cylindrical glass vessels of different diameter were available. Furthermore, for the same diameter, two different types of vessel were at hand: one with smooth wall and the other one with 18 small flower-baffles, like in Figure 2.2. The vessel with smooth wall is easily convertible to a baffled vessel by placing the baffles at the walls, as shown in Figure 4.14.

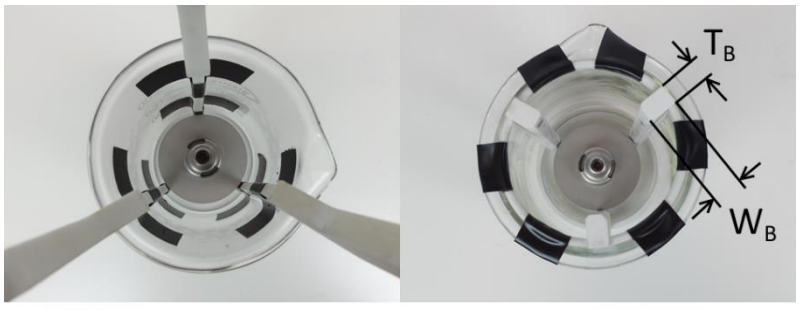

$D_{RB}/D_V = 0.85$ $D_{RB}/D_V = 0.71$

Fig. 4.14. *Two of the vessels with normal baffles used.*

Using the RB as stirring element, the effect of the baffles type on the reaction time was studied for all the different diameters available.

For each diameter, a different liquid volume was used in order to keep the ratio H_L/D_V at a constant value of 1.2 approximately. For the vessel without baffles with $D_{RB}/D_V = 0.85$ a higher H_L/D_V value was needed to avoid the entrance of air inside the RB through the superficial vortex (with the mechanism explained at the beginning of § 4.3.3), occurring even with the RB kept at the bottom of the vessel if H_L is lower than 1.64. That's why $H_L/D_V = 1.64$ for $D_{RB}/D_V = 0.85$.

The resin amount and the NaOH injection volume were changed proportionally to the liquid volume, using this reference: 5 mL of resin for 200 mL of liquid and injections of 100 µL of NaOH 1.05 M solution.

For a better understanding of the geometry and a better analysis of the results, the vessel diameter is expressed as the ratio of the RB diameter and the vessel diameter, D_{RB}/D_V, and the height of the liquid as the ratio H_L/D_V. The baffle types are indicated with the acronyms NB (normal rectangular baffles) and FB (flower baffles). When no baffles are used the acronym is S (smooth wall).

During each test, the height of the rotating bed was varied, like in the experiment of § 4.3.3.

The data and the pictures of the experiments made are reported in Table 4.4 and Figure 4.15 respectively. The characteristic of the normal rectangular baffles used are reported in Figure 4.14 and Table 4.4.

Table 4.4. *List of the experiments and experimental conditions.*

D_{RB}/D_V	H_L/D_V	Baffles type	V_L [mL]	V_R [mL]	V_{NaOH} [µL]	RS [rpm]	H_{RB} tested [mm]	NaOH inj. for each height
0.85	1.64	S	190	4.8	95	500	4	15
0.85	1.64	FB	190	4.8	95	500	45, 30, 15, 0	4
0.71	1.22	S	220	5.5	110	500	4	15
0.71	1.22	NB, FB	220	5.5	110	500	27, 18, 9, 0	4
0.62	1.25	S	340	8.5	170	500	4	15
0.62	1.25	NB, FB	340	8.5	170	500	39, 26, 13, 0	4
0.48	1.10	S	650	16.3	325	500	4	15
0.48	1.10	NB, FB	650	16.3	325	500	48, 32, 16, 0	4

Figure 4.15. *Set-up of the various experiments made with vessels of different diameter and different types of baffles.*

When vessels without baffles are used, a very deep vortex is formed at the liquid surface when the RB rotates, as shown in Figure 4.16 and as expected. If the RB is too high, the center of the vortex touches the holes on the top of it and air enters in the RB towards them. That is why the RB must be kept very close to the bottom and is not possible to vary its height in the experiments without baffles, as clear from Figure 4.16.

Table 4.4. *Dimensions of the rectangular baffles used in the different vessels.*

D_{RB}/D_V	Type of baffles	Number of baffles	T_B [mm]	W_B [mm]
0.71	Normal baffles	3	4	8
0.62	Normal baffles	3	8	12
0.48	Normal baffles	3	7	12

Figure 4.16. *Influence of the baffles on the dimension of the vortex which is formed when the RB is rotating.*

In Figure 4.16 is also shown that normal and flower baffles dramtically recude the surface vortex formation. This allows to keep the RB very close to the liquid surface and to test different heights of the RB.

With the smallest diameter vessel (D_{RV}/D_B = 0.85) the space between the external surface of the RB and the wall of the vessel was very small and it was not possible to insert the normal baffles. Only the flower-baffles were tested. Here an advantage of the flower-baffles comes out: with them the volume of the reactor is better exploited and is possible to use bigger internals or a bigger RB.

The procedure used for each experiment was the same used for the two experiments of §4.3.3. Each experiment was started with 4 NaOH injections keeping the RB at the maximum height, than the height was decreased gradually. 4 NaOH injections were made per each height.

Each experiment was repeated two times and the results of the two replications were the same. For this reason only one of the two replicas is reported in the results.

The results are reported in Figure 4.17 in two modalities:

- the reaction times as function of RB height and the NaOH injections;
- the mean value of the reaction times obtained as function of the height.

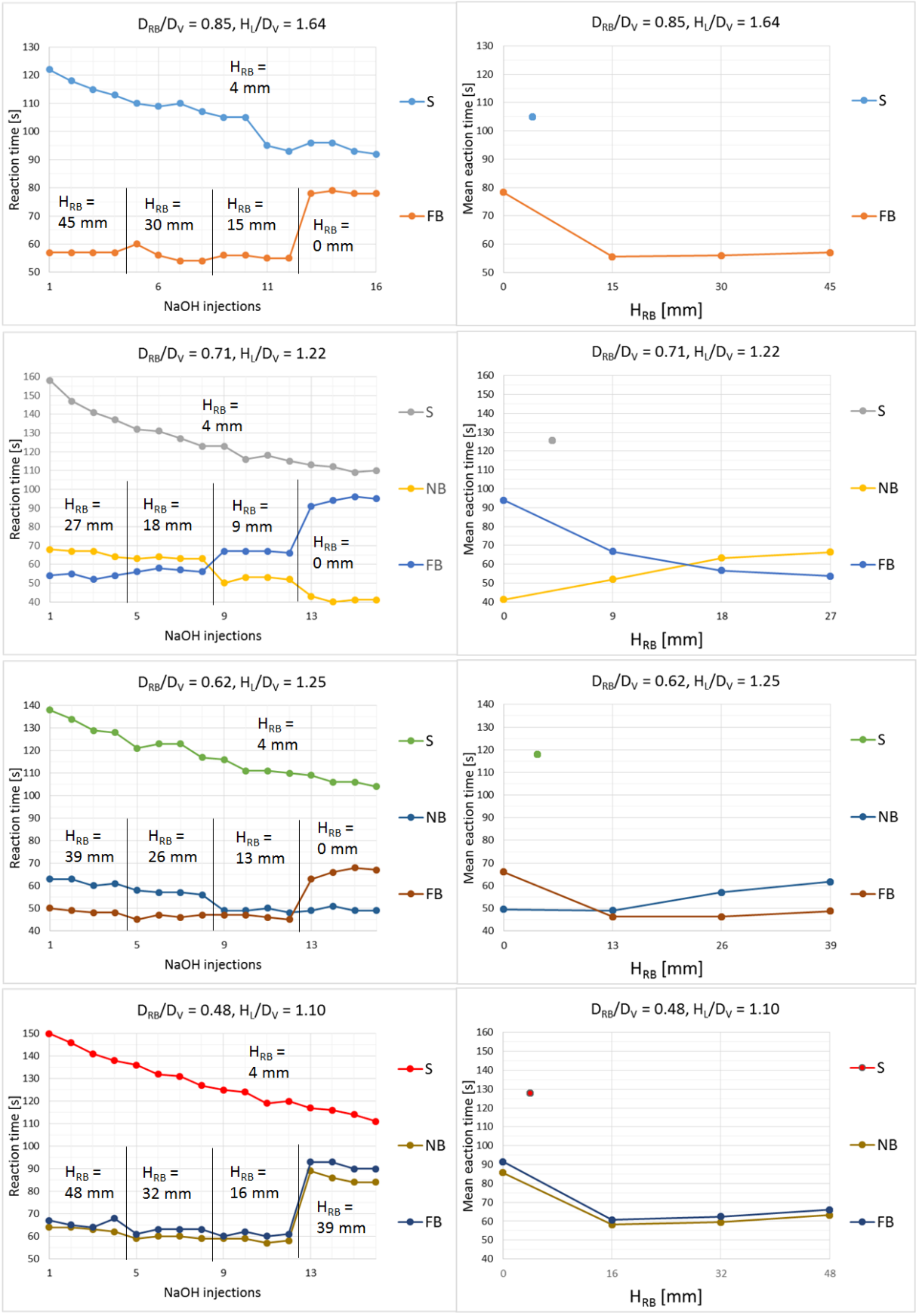

Figure 4.17. *Reaction times obtained with vessels of different diameter and types of baffles, as a function of the RB height and NaOH injections.*

First of all is clear that when no baffles are employed, the reaction time is much larger than any other case.

With flower-baffles, the trend of the reaction time as function of the height, for vessels of different diameter, is the following:

- with D_{RV}/D_B = 0.85, 0.62 and 0.48 the reaction time is not much influenced by the height as far as the rotating bed is not too close to the bottom of the vessel. Then the reaction time increases considerably;
- with D_{RV}/D_B = 0.71 the reaction time is more dependent to the height of the bed and the two variables are always inversely proportional.

On the contrary, with three normal baffles the reaction time is directly proportional to the height of the rotating bed for D_{RV}/D_B = 0.71 and 0.62. For D_{RV}/D_B = 0.48 the behaviour and the values of the reaction times are equal to those obtained with flower baffles.

The cause of this phenomena could be that the normal baffles improve the mixing of the liquid above the RB when they are very close to the lateral surface of it, as they were in the cases of D_{RV}/D_B = 0.71 and 0.62 (Figure 4.14). It was supposed that the liquid discharged from the lateral surface of the RB impacts on the big baffles and is forced to split, partly in the upper, partly in the lower region of the vessel, improving the mixing above the RB.

Since the two types of baffles have an opposite influence on the reaction time when the height of the RB is modified (except with D_{RV}/D_B = 0.48), it is difficult to say which one is the best by looking only at these experiments. Furthermore, the fact that the reaction time naturally decreases with the number of NaOH injections makes the comparison even more difficult.

To assess which type of baffles is better the comparison should be done as:

- find the optimum height of the RB for both vessels with different baffles first;
- keeping the RB at the optimum height, compare the performances of the vessels with the different type of baffles.

Probably for D_{RV}/D_B = 0.85 the normal baffles are equal to the flower baffles because the RB is far from the baffles and its interaction with them is very weak, without differing between the two types of baffles. This explains also the fact that the dependence of the reaction time on the RB height is almost nil, except when the RB is very low and the interactions with the bottom of the vessel becomes important.

Chapter 5

Conclusions

The aim of this project was to investigate the performances of the SpinChem® rotating bed reactor (RBR) and compare it with a normal stirred tank reactor (STR). The influence of some geometrical parameters such as the vertical position (height) of the RB in the vessel, the type of baffles and the vessel diameter has been investigated too.
Two solid-liquid non-catalytic reactions were used for this purpose: the scavenging of a genotoxic impurity and an ion-exchange reaction.

The scavenging of genotoxic impurites chosen consisted in the removal of impurities of 2-cyclohexen-1-one (genotoxic impurity) from the product to purify, cyclohexanone, by means of a solid thiol scavenger. The scavenger used was made of fused-silica spherical particles functionalized with thiol-propane groups and was available in three different particle sizes. Only few studies about this type of reaction were found in the literature, hence was necessary to optimize the reaction conditions.
It was found that the reaction takes place only if a non-nucleophilic basic catalyst (like N,N-diisopropylethylamine) is added to the solution and a very large excess of scavenger is employed (more than five equivalents with respect the initial moles of 2-cyclohexen-1-one). Nevertheless, the reaction is quite slow and usually more than 24 hours are needed to arrive at a final concentration of a few dozen of ppm of the impurity. If an alcoholic solvent is used instead of the cyclohexanone, the reaction is comparatively faster and is possible to arrive at a final concentration of 2-cyclohexen-1-one lower than 10 ppm after 24 hours using a reasonable excess of scavenger. Still, the reaction remains faily slow so that neither the type of reactor, nor the rotation speed influence the reaction rate. It means that the controlling regime is not the external mass transfer. It was found that the reaction rate is inversely proportional to the particle size of the scavenger. This could be due to a resistance caused by the internal mass transfer inside the pores, as it suggested by the reaction modelling.

The second reaction studied is the removal of sodium hydroxide from an aqueous solution with a cation exchange resin. In this case the reaction time can be significantly influenced by the rotation speed and the reactor type. Above 400 rpm the RBR was always more effective than

the STR. It can be concluded that the reaction is external mass-transfer limited and the RBR effectively improves the external mass transfer when the rotation speed is high enough.
Since the reaction is externally mass transfer limited, we studied the effect of other variables affecting the internal mixing, on the reaction time: the vertical position (height) of the RB in the vessel, the type of baffles and the vessel diameter.
In vessels without baffles a deep vortex is created, increasing the reaction time. Among the normal rectangular baffles and the flower baffles it was not possible to states uniquely which one is the best and further studies are needed for that.
It was found that also the distance between the RB and the vessel bottom (height) influences the reaction time. In vessels with normal baffles the reaction time is directly proportional to the height. In vessels with flower baffles is the opposite: the two variables are inversely proportional. In this last case the reaction time is weakly affected by the height if the RB is not too close to the bottom. Then the reactor is much less effective.
These considerations hold when the vessel diameter is small enough, compared to the RB diameter, and there are strong interactions between the RB and the wall of the vessel. When the diameter of the vessel is large, the behavior obtained with the normal baffles is equal to that of the flower baffles and also the reaction time is the same.

Concluding, it is important to remark that only if a reaction is externally mass-transfer limited the RBR can give advantages with respect to a normal STR. If this is the case, before comparing the two reactors, an individual optimization (to find for example the optimum height of the stirring element) should be carried out for each type of reactor.
In this work the comparison of the two reactors was done employing a vessel with flower baffles, before the discovery of the effect of the RB position on the reaction time. It would be interesting to repeat this comparison:

- with the RB and the impeller at their optimum height.
- with the RB and the impeller at the optimum height, using the normal baffles instead of flower baffles.

Notation

$\dot{n}_A^{b\to i}$	molar flux of species A, per unit volume of liquid, from the bulk to the external interface of the solid
$h_{m,A}$	external mass transfer coefficient of species A
C_A^b	concentration of species A in the bulk of the liquid
C_A^i	concentration of species A adjacent to the external surface of the solid
$a^{L,i}$	interfacial area of the solid, per unit volume of liquid, available for the external mass transfer
A^i	external area of the solid (excluding the area given by the solid porosity)
V^L	total volume of liquid
R''	reaction rate per unit area of the solid
υ_A	stoichiometric coefficient of species A
r_A''	reaction rate of species A
$a^{L,tot}$	total area of solid per unit volume of liquid
A^{tot}	total solid surface in the reactor
R'''	reaction rate per unit of volume of solid (including the volume of the pores)
$a^{S,tot}$	total area of solid per unit volume of solid (including the volume of the pores)
$\mathfrak{D}_e$	effective diffusion coefficient
k'''	kinetic costant referred to the reaction rate per unit of volume of solid (including the volume of the pores)
k''	kinetic costant referred to the reaction rate per unit area of the solid
L	characteristic length of the solid particles
n	reaction order
d_p	particle diameter
$\mathfrak{D}_{A,L}$	diffusion coefficient of species A in the liquid solution
$(r_A)_{obs}$	reaction rate of A observed experimentally
ρ_p	density of the solid particle, based on the volume of the particles (including the volume of the pores)
m_S	mass of solid
$V^{p,tot}$	total volume of the solid particles (including the volume of the pores)
S_a	total area of solid per unit mass of solid
V_L	liquid volume
V_R	resin volume
V_{NaOH}	injection volume of NaOH 1.05 m
RS	rotation speed

H_{RB}	height of the rotating bed base from the vessel bottom
H_I	height of the impeller base from the vessel bottom
H_L	liquid height in the reactor
D_L	vessel diameter
D_{RB}	rotating bed diameter

Greek letters

ϕ	Thiele modulus
η	effectiveness factor
ε_p	particle porosity
τ	solid tortuosity

Acronyms

RBR	rotating bed reactor
RB	rotating bed
STR	stirred tank reactor
PBR	packed bed reactor
GI	genotoxic impurity
API	active pharmaceutical ingredient
TS	thiol scavenger
TG	thiol groups
DIEA	N,N-diisopropylethylamine
B	basic catalyst
spv	specific pore volume

Bibliography

1. Balu, N., Padgett, W., Lambert, G., Swank, A., Richard, A. and Nesnow, S. (2004). Identification and Characterization of Novel Stable Deoxyguanosine and Deoxyadenosine Adducts of Benzo[a]pyrene-7,8-quinone from Reactions at Physiological pH. Chem. Res. Toxicol., 17(6), pp.827-838.

2. Bruice, P. (2004). Organic chemistry. Upper Saddle River, NJ: Pearson/Prentice Hall.

3. Controlled Chemicals, Inc., Colmar, PA (US), (2015). PROCESS FOR REDUCING CONTAMINATING MICHAEL ACCEPTOR LEVELS IN OXYCODONE AND OTHER COMPOSITIONS. US 7,875,623 B2.

4. Fogler, H. (2005). Elements of chemical reaction engineering. Prentice Hall PTR.

5. Jouyban, A. and Pars, H. (2012). Genotoxic Impurities in Pharmaceuticals. Toxicity and Drug Testing.

6. Khatik, G., Kumar, R. and Chakraborti, A. (2006). Catalyst-Free Conjugated Addition of Thiols to α,β-Unsaturated Carbonyl Compounds in Water. ChemInform, 37(40).

7. Krishnaveni, N., Surendra, K. and Rao, K. (2005). Study of the Michael Addition of β-Cyclodextrin—Thiol Complexes to Conjugated Alkenes in Water. ChemInform, 36(22).

8. Levenspiel, O. (1999). Chemical reaction engineering. New York: Wiley.

9. Li, G., Randev, R., Soeriyadi, A., Rees, G., Boyer, C., Tong, Z., Davis, T., Becer, C. and Haddleton, D. (2010). Investigation into thiol-(meth)acrylate Michael addition reactions using amine and phosphine catalysts. Polym. Chem., 1(8), p.1196.

10. Mather, B., Viswanathan, K., Miller, K. and Long, T. (2006). Michael addition reactions in macromolecular design for emerging technologies. Progress in Polymer Science, 31(5), pp.487-531.

11. Michael addition of thiols to α,β-unsaturated carbonyl compounds under solvent-free conditions. (2006). Arkivoc, 2006(12), p.130.

12. Missen, R., Mims, C. and Saville, B. (1999). Introduction to chemical reaction engineering and kinetics. New York: J. Wiley.

13. Müller, L., Mauthe, R., Riley, C., Andino, M., Antonis, D., Beels, C., DeGeorge, J., De Knaep, A., Ellison, D., Fagerland, J., Frank, R., Fritschel, B., Galloway, S., Harpur, E., Humfrey, C., Jacks, A., Jagota, N., Mackinnon, J., Mohan, G., Ness, D., O'Donovan, M., Smith, M., Vudathala, G. and Yotti, L. (2006). A rationale for determining, testing, and controlling specific impurities in pharmaceuticals that possess potential for genotoxicity. Regulatory Toxicology and Pharmacology, 44(3), pp.198-211.

14. Paul, E., Atiemo-Obeng, V. and Kresta, S. (2004). Handbook of industrial mixing. Hoboken, N.J.: Wiley-Interscience.

15. Poling, B., Prausnitz, J. and O'Connell, J. (2001). The properties of gases and liquids. New York: McGraw-Hill.

16. Schmidt, L. (1998). The engineering of chemical reactions. New York: Oxford University Press.

17. Schmidt, T., Lyß, G., Pahl, H. and Merfort, I. (1999). Helenanolide type sesquiterpene lactones. Part 5: The role of glutathione addition under physiological conditions. Bioorganic & Medicinal Chemistry, 7(12), pp.2849-2855.

18. Shi, B. and Greaney, M. (2005). Reversible Michael addition of thiols as a new tool for dynamic combinatorial chemistry. Chemical Communications, (7), p.886.

19. Wikipedia, (2015). Non-nucleophilic base. [online] Available at: https://en.wikipedia.org/wiki/Non-nucleophilic_base [Accessed 30 Nov. 2015].

20. P. A. Sarathi, C. Gnanasekaran, and A. Shunmugasundaram (2008). Kinetics and Mechanism of Triethylamine Catalysed Michael Addition of Benzenethiol to 1-(2-Nitrovinyl)benzene in Acetonitrile. Bull. Korean Chem. Soc., Vol. 29, No. 4

21. Barahman Movassagha,b and Pershang Shaygana (2006). Michael addition of thiols to a,ß-unsaturated carbonyl compounds under solvent-free conditions. General Papers ARKIVOC 2006 (xii) 130-137

22. GENOTOXIC IMPURITIES IN PHARMACEUTICAL PRODUCTS (2013). © Agilent Technologies, Inc..